ASD-TDR-63-506

FLUID MECHANICS AND TANKAGE DESIGN FOR LOW GRAVITY ENVIRONMENT

Robert G. Clodfelter

TECHNICAL DOCUMENTARY REPORT NO. ASD-TDR-63-506

September 1963

AF Aero-Propulsion Laboratory
Research and Technology Division
Air Force Systems Command
Wright-Patterson Air Force Base, Ohio

Project No. 3141, Task No. 314105

NOTICES

When Government drawings, specifications, or other data are used for any purpose other than in connection with a definitely related Government procurement operation, the United States Government thereby incurs no responsibility nor any obligation whatsoever; and the fact that the Government may have formulated, furnished, or in any way supplied the said drawings, specifications, or other data, is not to be regarded by implication or otherwise as in any manner licensing the holder or any other person or corporation, or conveying any rights or permission to manufacture, use, or sell any patented invention that may in any way be related thereto.

Qualified requesters may obtain copies of this report from the Defense Documentation Center (DDC), (formerly ASTIA), Cameron Station, Bldg. 5, 5010 Duke Street, Alexandria 4, Virginia

This report has been released to the Office of Technical Services, U.S Department of Commerce, Washington 25, D.C., in stock quantities for sale to the general public.

Copies of this report should not be returned to the Aeronautical System Division unless return is required by security considerations, contractual obligations, or notice on a specific document.

FOREWORD

This report was prepared to present the results of an in-house study and test program conducted by the AF Aero-Propulsion Laboratory, Aeronautical Systems Division, under Project 3141, "Electric Propulsion Technology," Task 314105, "Space Environmental Effects on Electric Propulsion." The report covers the effort between June 1961 and April 1963.

The cooperation and assistance of the many persons who have contributed to the program and specifically to the following individuals of the AF Aero-Propulsion Laboratory are gratefully acknowledged: SM/Sgt C. W. Thompson for coordinating the experiments and acting as aircraft test monitor for the program during the past 4 years; Elmer White for developing the 7090 computer program to determine interface shapes; and P. J. Vore and G. N. Medisch for developing the drop tower into a useful zero-gravity test facility.

ABSTRACT

Electric propulsion systems for space vehicles must be able to restart and operate at zero and low gravity. This operation can be achieved if the tankage delivers only single-phase propellants. The requirements for feed systems of electric engines are described briefly. Also, the 1.85-second drop-test facility is described and the testing techniques are discussed.

The minimum energy principle is presented along with a method for determining the direction of mass transfer in tapered tubes and liquid-vapor interface shapes in an annular space between concentric cylinders. Possible feed systems for electric engines are given, which utilize surface tension for fluid positioning and transfer.

Zero-gravity and static-fluid configurations in cylindrical and spherical containers are discussed along with experimental observations. The interface "overshoot" of the equilibrium zero-gravity configuration is also discussed.

PUBLICATION REVIEW

This technical documentary report has been reviewed and is approved.

FOR THE COMMANDER:

ROBERT E. SUTTON
Assistant Chief
Aero Space Power Division
AF Aero Propulsion Laboratory

TABLE OF CONTENTS

LIST OF ILLUSTRATIONS

LIST OF ILLUSTRATIONS (Continued)

INTRODUCTION

Electric propulsion systems for space vehicles must have both zero-gravity restart capability and low gravity (10^{-4} G's to 10^{-3} G's) operation capability. Smooth, reliable, and reproducible operation of the engine is essential and can be achieved only if single-phase propellants are delivered from the tankage.

In contrast to conditions on the surface of the earth, there can be no assurance that the desired propellant phase will be located at the outlet of the tank while the vehicle is in free fall or under very low accelerations.

This technical report* presents information on both the nature of fluids at low gravity and on tankage systems for electric engines, which control the propellant configuration by surface tension. This information is presented to assist designers in developing tankage systems that have many advantages over mechanical methods (rotating tanks, bladder expulsion, etc.) of fluid control at low gravity.

ELECTRIC ENGINES

TYPES OF ENGINES

The electric propulsion engines that are currently being considered for space application are listed in ascending order of specific impulse range: (1) resistance engines, (2) arc-jet engines, (3) electromagnetic engines, and (4) electrostatic engines.

The electrothermal resistance engine shows promise in the 800-second to 1100-second specific-impulse range. In this engine, the propellant is heated by a resistance heat exchanger of refractory metal; the maximum temperature of the propellant and, therefore, specific impulse is limited by the maximum temperature of the resistance element. The electrothermal arc-jet engine produces greater specific impulses because the propellant is heated by an electric arc without subjecting the structural elements to the maximum temperature of the propellant. The electromagnetic engine produces thrust by the interaction of a neutral, but electrically conducting, plasma propellant with electromagnetic fields. Since the propellant is accelerated by both aerodynamic means and electric body forces, a greater specific impulse is associated with the same maximum allowable temperature of the propellant than with the arc-jet engine. The electrostatic engine (ion engine) operates in the 5000-second to 20,000-second specific-impulse range. This engine produces thrust almost solely by accelerating charged particles by electrical means. Here, there is almost complete decoupling of the maximum attainable velocity of the exhaust and operating temperature of the structural components. Since the arc-jet and electrostatic engines are closest to becoming operational, only these are included in the discussion on the requirements for propellant feed systems.

---

*A 16-mm film which supplements the information presented in this report can be obtained on loan by contacting the author.

Manuscript released by author on 21 May 1963 for publication as an ASD Technical Documentary Report.

FEED SYSTEM REQUIREMENTS

At the present time, the selection of the propellant for the arc-jet engine probably will be limited to ammonia, hydrogen, and the lithium seeded versions of each. Ammonia is easily stored in a no-loss system and as such offers weight advantages for long term storage in space. Hydrogen while being superior to ammonia from the standpoint of engine performance requires cryogenic or supercritical storage techniques and no-loss systems are impractical for long term storage in space. On a mission where hydrogen boil-off supplies the fuel required by the engine, hydrogen definitely appears to be the logical choice between the two. Although the arc-jet engine will operate on either a liquid or gas propellant, the feed control system, from a practical standpoint, requires the propellant to be in the gaseous state.

Cesium is easily stored as a liquid in a no-loss system and could be stored as a solid with or without a refrigeration system depending on the heat balance of the tank. With the cesium propellant, the critical requirements are the compatibility of the cesium with the tank materials and the purity of the cesium delivered to the engine. Gaseous cesium must be delivered to the emitter (ion generator) for proper operation.

Before the high-performance potential of electric engines can be fully realized, these engines must have an efficient method of propellant storage. In addition to the environmental problems encountered in space that are common to other propulsion systems, electric engines will be required to perform in a low-gravity environment (less than 10^{-3} G's) during their entire operational period, which may be as high as 3 years. This low-gravity environment presents problems in liquid-vapor separation and heat-transfer processes. In recent years much effort has been devoted to the analysis of these problems. Many different systems have been investigated (Refs. 1 through 16). The general conclusion was that a system could be developed that offered many distinct advantages in weight, power, and simplicity over present state-of-the-art techniques of propellant storage if fluid positioning could be obtained by natural means (Van der Waals forces). The efforts described in References 1 through 16 were directed primarily toward the development of propellant storage techniques for near future applications. Since there was a lack of design information on the behavior of fluids in a low-gravity environment, less desirable techniques were selected for development. The intent of this report is to present some information on low-gravity fluid behavior so that the full potential of advanced concepts of propellant storage may be realized at some future date.

SURFACE TENSION SYSTEMS

From principles of thermodynamics, we can show that an isolated physical system will tend to assume a state of minimum energy equilibrium. For a system involving fluids, the energy may be dissipated by irreversible action of viscosity, capillary friction, and heat transfer. For fluid in a container under an a G's acceleration, the energy of the system that may be minimized is the energy associated with the liquid-solid, liquid-vapor and vapor-solid interfaces plus the potential energy associated with accelerated fluid. Using this principle, the authors of References 17 through 19 predict liquid-vapor interface shapes in various types of containers and acceleration fields. The constraints for a system in a zero-gravity environment ($a = 0$) is a liquid-vapor interface of constant curvature intersecting the container at the contact angle.

The Young and Laplace equation (Ref. 20), which deals with the pressure differential across a curved interface, is a useful tool for predicting the behavior of low-gravity fluid. This basic equation of capillarity is

$$P_0 - P_1 = \sigma \left(\frac{1}{R_1} + \frac{1}{R_2} \right)$$

where

$P_0 - P_1$ = pressure differential across liquid-vapor interface

σ = surfaced tension

R_1 and R_2 = radii of curvature that describes the curved interface.

The two radii of curvature of a curved surface may be obtained by erecting a normal to the surface at the point in question and then pass a plane through the surface containing the normal. The radius of curvature is that of a circle tangent to the line of intersection at the point involved. The second radius of curvature is obtained in the same manner by passing a second plane through the surface containing the surface normal but perpendicular to the first plane. The ΔP across an interface cannot depend upon the manner in which the two radii of curvature are chosen; therefore, R_1 and R_2 need not necessarily be the principal radii of curvature. R_1 or R_2 are considered positive if they lie on the P_0 side of the curved surface.

The pressure drop across a liquid-vapor interface may be utilized for mass transfer. Consider the simple example of slightly tapered tube (shown in Figure 1).

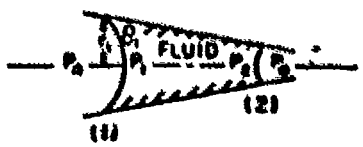

Figure 1. Slightly Tapered Tube

$$P_0 - P_1 = \sigma_1 \left(\frac{2}{r_1} \right) \cos \theta_1$$

and

$$P_0 - P_2 = \sigma_2 \left(\frac{2}{r_2} \right) \cos \theta_2$$

where

θ = contact angle

and

r = tube radius.

Combining these two equations gives

$$\frac{P_1 - P_2}{2} = \sigma_2 \frac{\cos \theta_2}{r_2} - \frac{\sigma_1}{r_1} \cos \theta_1$$

Now if

$$\frac{\sigma_2 \cos \theta_2}{r_2} > \frac{\sigma_1 \cos \theta_1}{r_1} ,$$

the fluid moves to the right, and if

$$\frac{\sigma_2 \cos \theta_2}{r_2} < \frac{\sigma_1 \cos \theta_1}{r_1} ,$$

the fluid moves to the left.

The relationship of the surface tensions, contact angles, and tube radii may be adjusted so that the fluid may be made to move in the desired direction. The surface tension and contact angle may be varied by the use of additives, impurities, or temperature. Figure 2 illustrates fluid movement for various conditions. Here, the surface tension decreased with increasing temperature is assured in the figure. This fact is true for most liquids. As the gravity environment becomes smaller, capillary tubes may be increased to several inches in diameter. Therefore, the overall weight of a storage system is reduced when this principle for propellant control is used.

When the idea of mass transfer by surface tension is used, several possible tank systems may be postulated. For example see Figure 3. Figure 3a shows a tapered tank with a transfer line connecting the two tank ends. A wetting fluid will tend to collect at the small end of the tank regardless of the initial fluid configuration. Another type of tank is shown in Figure 3b. This tank consists of several concentric cylinders. When these cylinders are sized correctly, the liquid can be collected in the center portion of the tank with the ullage in the outer-most annular space. This effect could be used to reduce the heat leak of the tank. This method will be discussed in more detail later on. Other tank concepts utilizing surface forces are given in Reference 21.

For very low feed-rate systems such as those associated with the electric engines, the capillary forces alone are sufficient to provide the fluid to the engine. In other words, no pump or pressure transfer system is required to maintain the proper feed rate. This factor is particularly attractive for the ion engine where the liquid cesium may be transferred from the tank to the vaporizer by surface tension only.

Figure 4 gives a possible tank configuration of the ion engine. Basically this feed system consists of a storage tank that has the inner walls coated with a porous sponge material (nickel, stainless steel, etc.). The outlet tube is filled with a fine porous sponge material. The outlet tube terminates in the vaporizer. Heat is radiated from an electric heater to the liquid-vapor interface located at the end of the outlet tube; therefore vapor is provided to the engine. The flow rate can be controlled by adjusting the power to the heater. Since the pores of the tank sponge are larger than those of the outlet-tube sponge, the propellant is transferred to the end of the outlet tube if the propellant in the tank is in contact with the tank sponge. Analysis of surface energies, and verified by many experiments conducted by ASD, NASA, and others, insures contact of the propellant with the tank sponge. In other words, all fluids that have contact angles other than 180 degrees will be wall bounded.

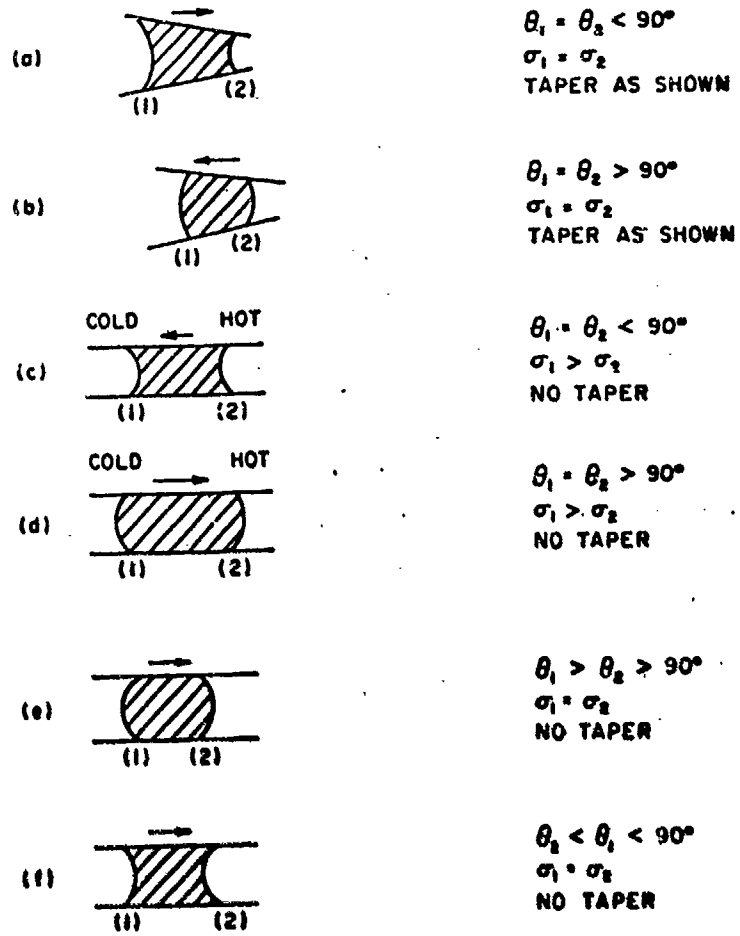

Figure 3. Fluid Movement in Capillaries

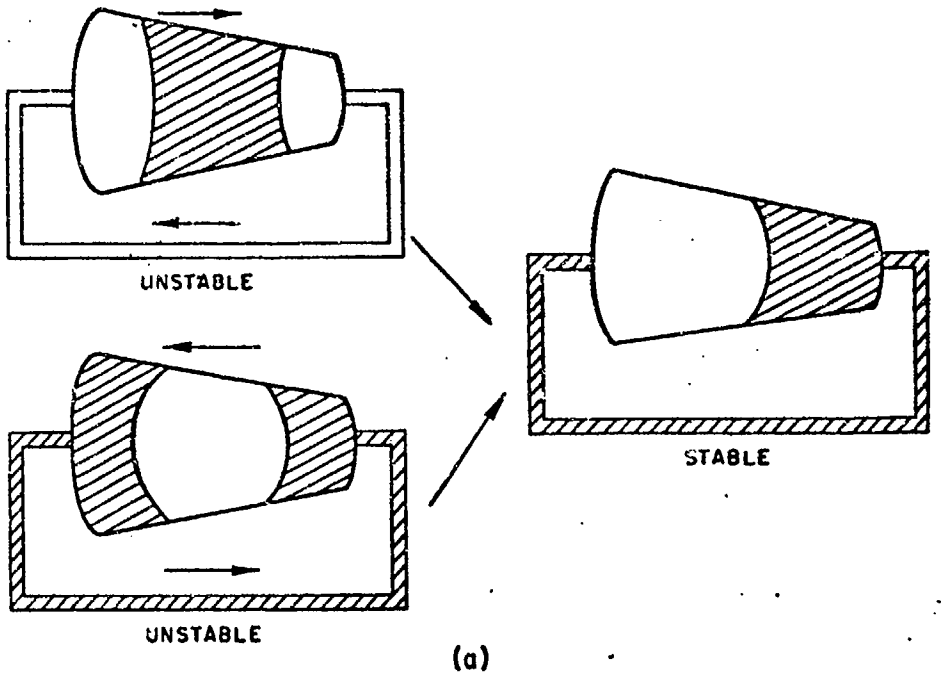

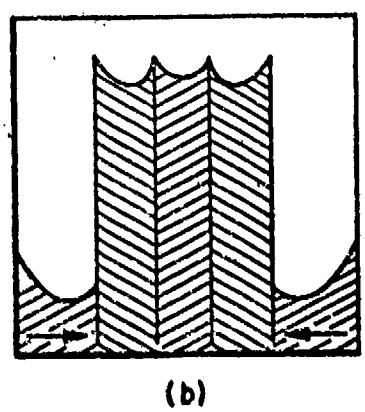

Figure 3. Low-Gravity Fluid Configurations Controlled by Surface Tension

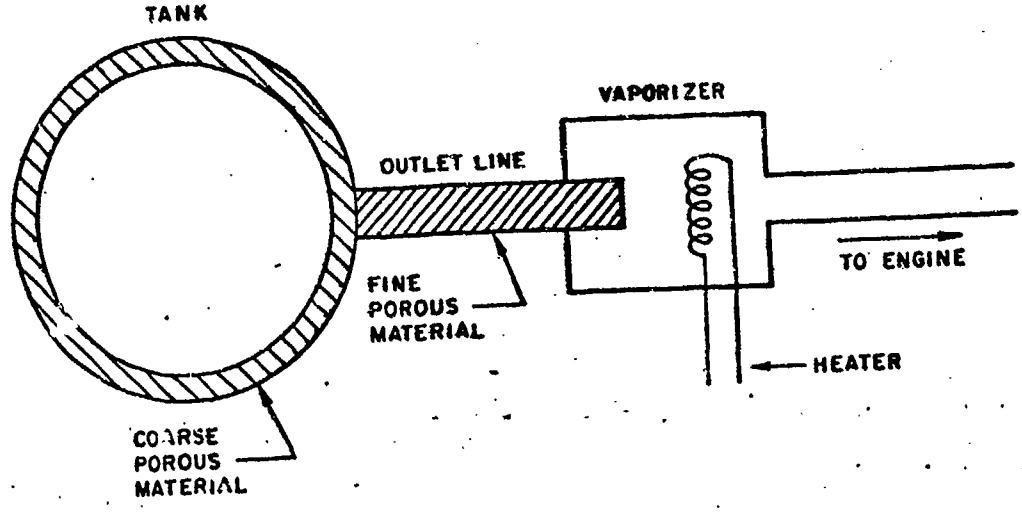

Figure 4. Feed System of Ion Engine

Note that the characteristic dimension of the vaporizer is less than the characteristic dimension of the tank. This means that the propellant would fill the vaporizer and vapor line in the absolute minimum surface-energy configuration. This problem may be overcome by either (1) lowering the characteristic dimension of the tank below that of the vaporizer or (2) by designing the vaporizer so that the propellant surface energy increases as the propellant leaves the outlet tube. In other words, the vaporizer presents an energy barrier to liquid that leaves the outlet tube.

For the arc-jet engine, it is desirable to use the heat leaks of the cryogenic storage tank to provide the vapor for the engine. Here the method is positioning the fluid and locating the feed line in the vapor region.

The control surfaces utilized for fluid positioning need not necessarily be of solid material. Screen may be used to reduce weight. When screen is used as a control surface, the stability of the fluid on the surface of the screen must be considered in the design. This problem is discussed in detail in Reference 22.

Two drop tests were conducted to illustrate the use of screens. Results of the tests are shown in Figure 5. Both tests utilized two Pyrex cylinders each with an inside diameter of 2.5 centimeters. Ethyl alcohol was used as the test fluid. One cylinder contained a 35-mesh screen and the other a 25-mesh screen standpipe. In Figure 5a, the standpipe diameter was 1 centimeter. For this arrangement, the motion of the liquid into the standpipe was predicted by the minimum energy principle. In Figure 5b, the standpipe diameter was 2 centimeters. Here the motion of the fluid was out of the standpipe. The variation of the interface in the annular space was the result of slight misalignment of the standpipe. A method of determining the direction of fluid motion and interface shape for an annular space is given in the section on Annular Capillary Analysis. These tests showed that in a capillary system the screen surface acted as a solid surface.

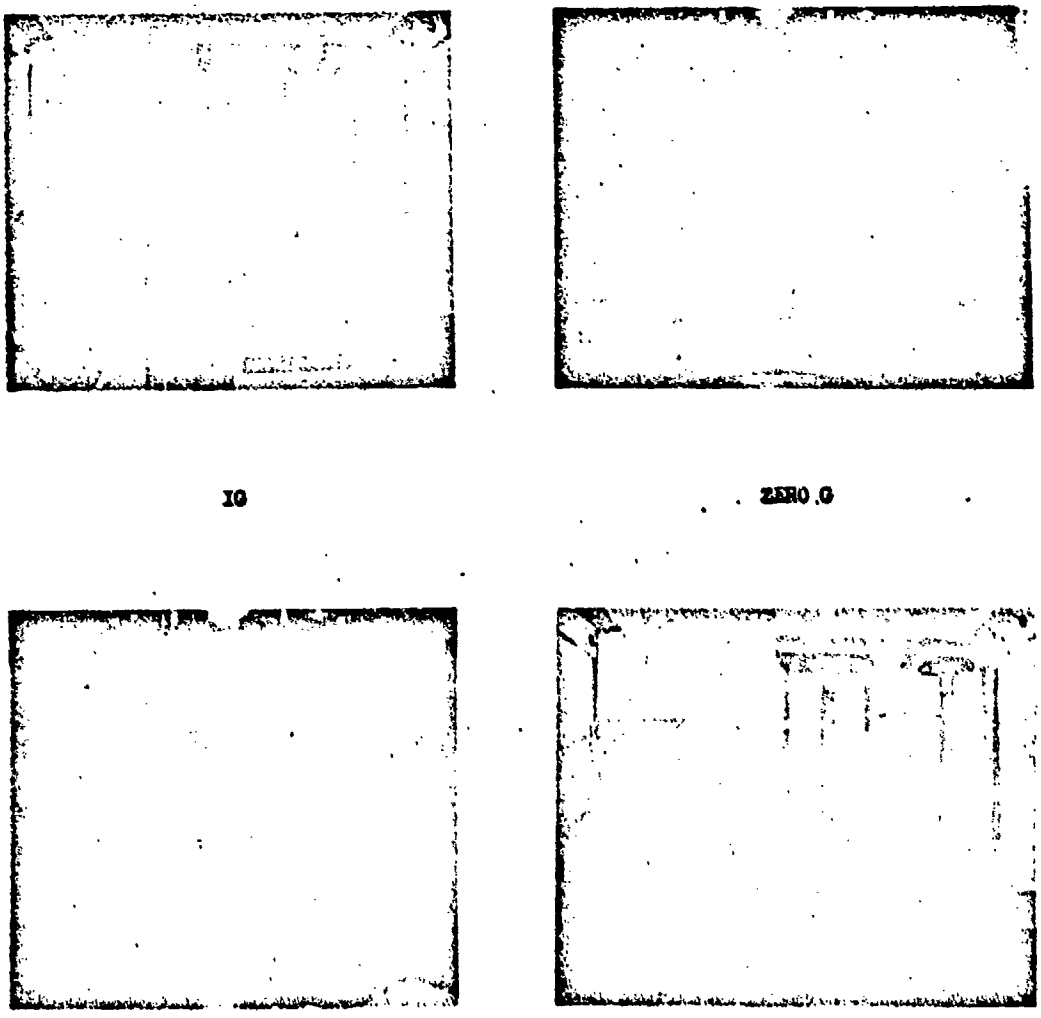

Figure 5. Screen Capillaries

ANNULAR CAPILLARY ANALYSIS

A sketch of a capillary system that will now be considered is shown in Figure 6.

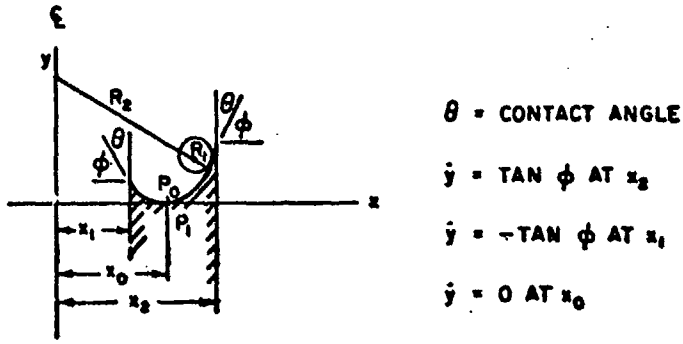

Figure 6. Capillary System

For figures or revolution, explicit expressions can be written for R_1 and R_2. From analytical geometry

$$\frac{1}{R_1} = \frac{\dot{y}}{(1+\dot{y}^2)^{3/2}}$$

and

$$\frac{1}{R_2} = \frac{\dot{y}}{x}(1+\dot{y}^2)^{1/2}$$

From the Young and Laplace equation

$$P_0 - P_1 = \sigma\left(\frac{1}{R_1} + \frac{1}{R_2}\right).$$

Let

$$\frac{P_0 - P_1}{\sigma} = k$$

and let

$$P = \dot{y}$$

$$\dot{y} = \frac{dP}{dx}$$

Now

$$k = \frac{P}{x(1+P^2)^{1/2}} + \frac{\frac{dP}{dx}}{(1+P^2)^{3/2}}$$

or

$$k\int x\,dx = \int \frac{P\,dx}{(1+P^2)^{1/2}} + \frac{x\,dP}{(1+P^2)^{3/2}}.$$

The integrand turns out to be the exact differential of

$$\frac{xP}{(1+P^2)^{1/2}}$$

so that

$$\frac{x^2}{2}\,k = \frac{xP}{(1+P^2)^{1/2}} + C.$$

From the boundary conditions

$$P = \tan\phi \quad \text{at } x_2$$
$$P = -\tan\phi \quad \text{at } x_1$$

and since

$$\phi = 90 - \theta,$$

we find

$$k = \frac{2\cos\theta}{x_2 - x_1}$$

and

$$C = \frac{x_2^2\,k}{2} - x\cos\theta.$$

These equations may be nondimensionalized by the substitution of

$$\bar{C} = \frac{C}{x_1}$$
$$\bar{k} = x_1 k$$
$$\bar{x}_0 = \frac{x_0}{x_1}$$
$$\bar{x}_2 = \frac{x_2}{x_1}$$
$$\bar{x} = \frac{x}{x_1}$$
$$\bar{y} = \frac{y}{x_1}$$

These equations now may be written as

$$\bar{C} = \frac{\bar{x}_2^2\cos\theta}{\bar{x}_2 - 1} - \bar{x}_2\cos\theta$$

and

$$\bar{k} = \frac{2\cos\theta}{\bar{x}_2 - 1}$$

Now the pressure drop across the interface may be determined as follows:

$$\Delta P = \sigma k = \frac{\sigma\, 2 \cos\theta}{(r_2 - r_1)}$$

Consider the system of concentric cylinders (Figure 7) if it is desired to drain fluid first from the outer annular space (3) then from annular space (2) and finally from tube (1).

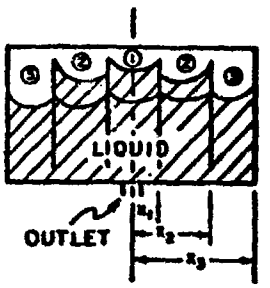

Figure 7. System of Concentric Cylinders

The necessary conditions are:

$$\Delta P_1 > \Delta P_2 > \Delta P_3$$

or

$$k_1 > k_2 > k_3$$

Substituting for

$$k_1,\ k_2,\ \text{and}\ k_3,$$

we find

$$\frac{\sigma\, 2 \cos\theta}{r_1} > \frac{\sigma\, 2 \cos\theta}{(r_2 - r_1)} > \frac{\sigma\, 2 \cos\theta}{(r_3 - r_2)}$$

Finally it is necessary that

$$r_2 > 2 r_1$$

and

$$r_3 + r_1 > 2 r_2$$

Surprisingly, the same results may be obtained simply by defining

$$\Delta P = \frac{F}{A} = \frac{\text{vertical force at the solid-liquid-vapor interface}}{\text{annular area}}$$

$$\Delta P_1 = \frac{2\pi r_1 \cos\theta}{\pi r_1^2} = \frac{2\sigma \cos\theta}{r_1}$$

$$\Delta P_2 = \frac{2\pi r_1 \sigma \cos\theta + 2\pi r_2 \sigma \cos\theta}{\pi r_2^2 - \pi r_1^2} = \frac{2\sigma\cos\theta}{r_2 - r_1}$$

and

$$\Delta P_3 = \frac{2\pi r_2 \sigma \cos\theta + 2\pi r_3 \sigma \cos\theta}{\pi r_3^2 - \pi r_2^2} = \frac{2\sigma\cos\theta}{r_3 - r_2}$$

The fact that the two techniques give the same results for this particular problem suggests the possibility that the pressure drop may be determined by the latter method for complex capillary systems, which cannot easily be found by rigid analysis. This concept is presently under investigation in the drop tower.

Now refer to the equation

$$\frac{r^2 k}{2} = \frac{rP}{(1+P^2)^{1/2}} + c,$$

by nondimensionalizing and rearranging gives

$$\frac{dY}{dR} = \frac{\left[\frac{R k}{2} - \frac{R}{k}\right]}{\left[1 - \left(\frac{R k}{2} - \frac{R}{k}\right)^2\right]^{1/2}}$$

since

$$\frac{dY}{dR} = 0 \text{ at } R_0$$

$$R_0 = \left(\frac{2}{k}\right)^{1/2}.$$

The shape of the interface may be determined by solving the preceding equation. Numerical solutions were calculated on a 7090 computer for various conditions.

Figure 8 gives the nondimensional interface shape for a wetting fluid ($\theta = 0°$) and Figure 9 deals with a nonwetting fluid $\theta = 125°$.

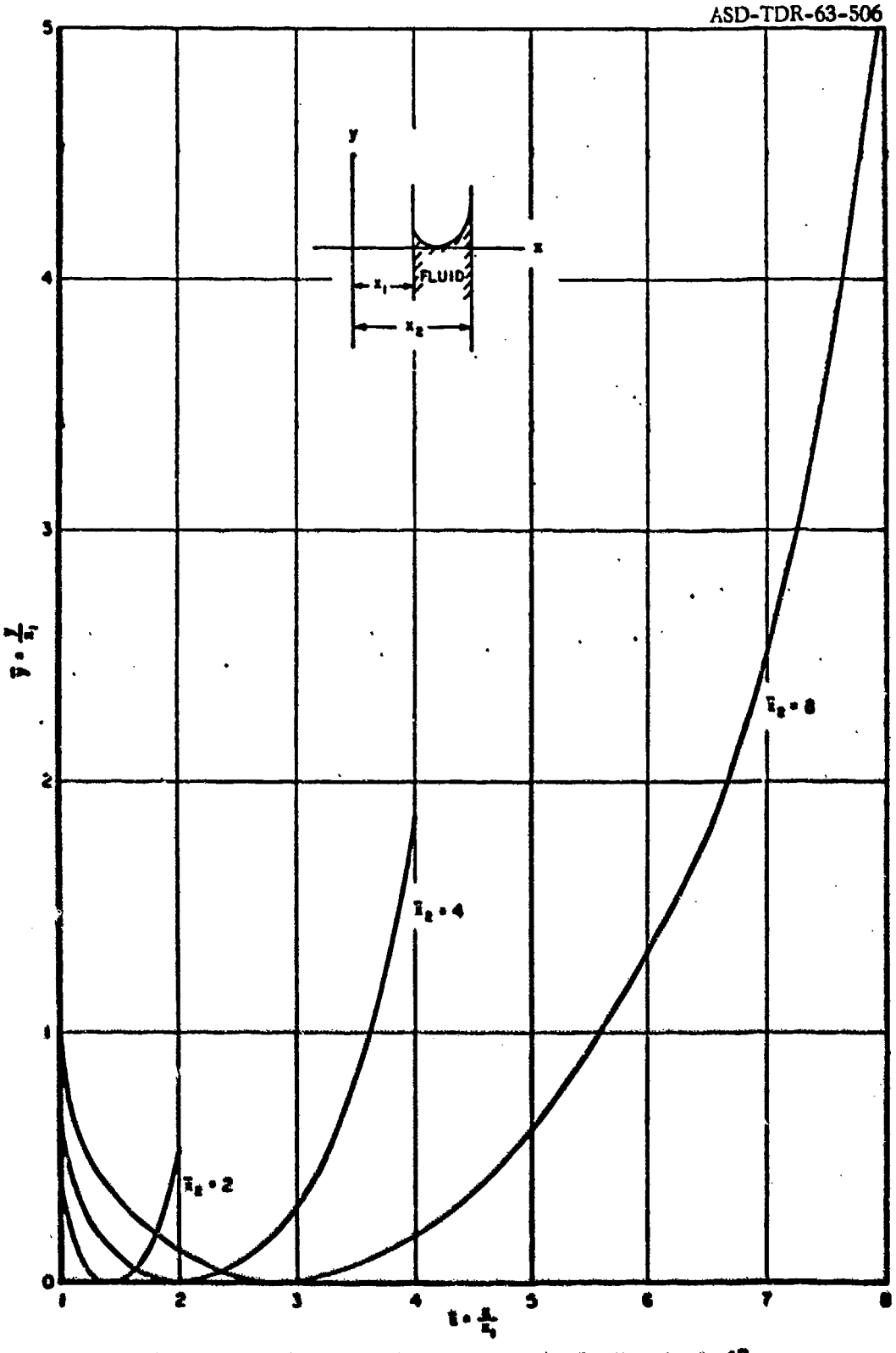

Figure 8. Nondimensional Interface in Annular Capillary for $\theta = 0^0$

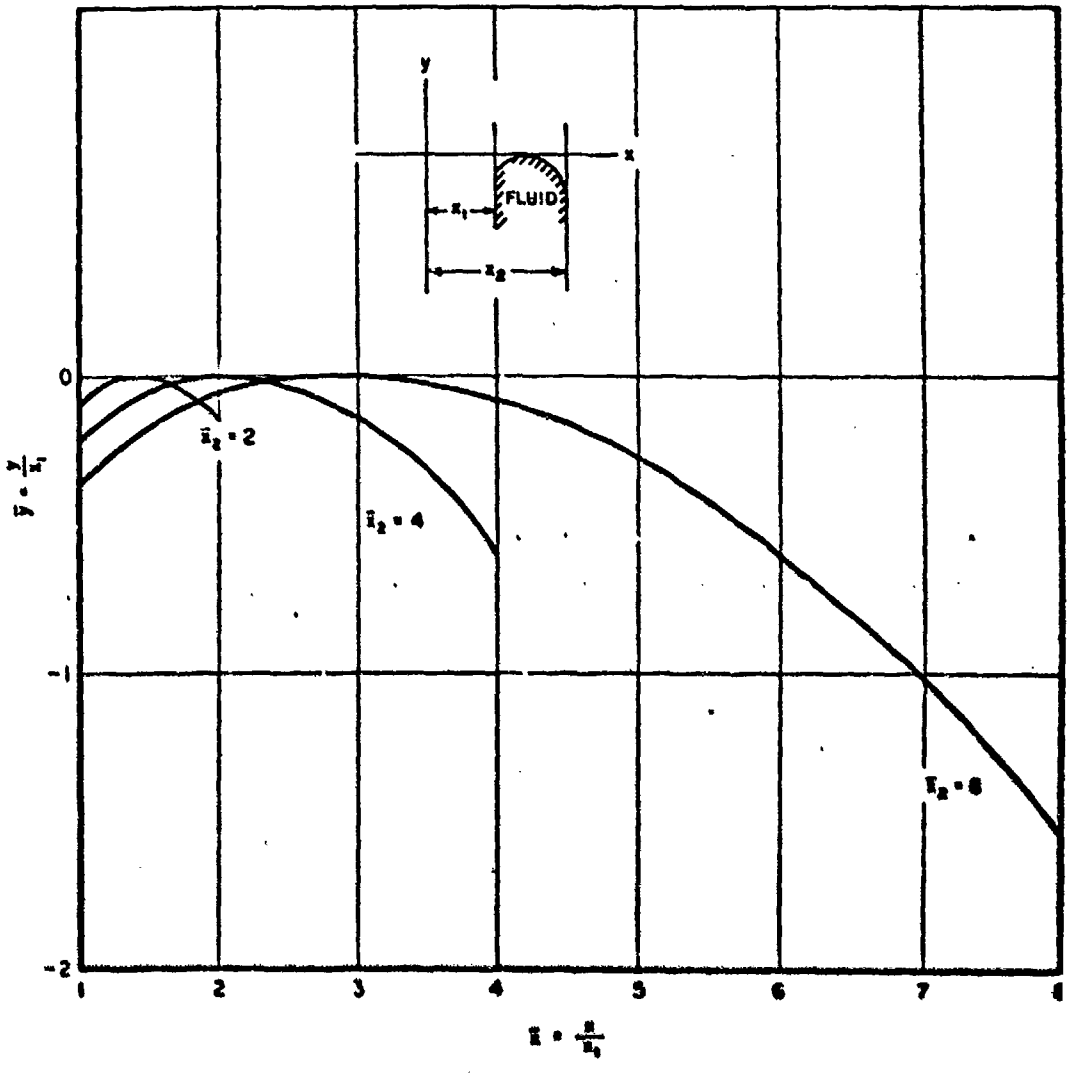

Figure 9. Nondimensional Interface in Annular Capillary for $\theta = 120^{\circ}$

ZERO-GRAVITY DROP FACILITY

The experimental methods used to investigate the effects of zero gravity must all apply the underlying principle that the apparatus experiencing zero gravity must be allowed to accelerate uniformly because of the influence of only the external force of gravity. Possible ways to apply this principle are given in Table 1. No one method can be used to provide all the information necessary. However, the drop method provides the most reliable and repetitive test conditions for the least amount of investment in manpower and money. Experience at ASD and other operational drop-test facilities substantiate the validity of results obtained from this method.

Past effort at ASD has centered around the aircraft method of producing the low-gravity test environment. The aircraft trajectory in many cases causes a fluid sloshing condition, which often distorts the phenomena under investigation. References 23 through 25 give the details of aircraft testing. Much qualitative information has been obtained from past aircraft testing. However, a drop facility was developed at ASD to enhance future aircraft testing, to provide quantitative data, and to investigate phenomena that could not successfully be determined from aircraft tests. The results presented in this report were obtained in this facility.

The drop facility has a usable drop height of 55 feet and yields free-fall time of 1.85 seconds. This drop facility is located in ASD Building 71B and is shown in Figure 10. The effect of air drag on the test package is kept to a minimum by allowing the test package to fall within a protective drag shield. Guide cables are used to facilitate positioning of the capsule assembly at the top of the shaft and to ensure that the capsules do not tip over after coming to rest at the bottom of the shaft.

A honeycomb paper material, developed by the Army for parachute drops and procured under Military Specification H9854, is used to absorb the kinetic energy of the capsules on impact. This paper is available in three strengths expressed in the force required to crush 1 square foot of the material. The 2800-pound per square foot paper is presently being used with the 300-pound capsule in the 1.8-second drop facility. The paper stack is shown in Figure 11.

By varying the cross sectional area of the honeycomb paper and selecting the correct strength of paper, one can control the G forces encountered at the bottom of the drop to prevent any damage to the experiment or instrumentation.

Various other methods of catching the capsule were studied, observed, and investigated. The preceding method has proved very satisfactory.

During the free-fall period, the air resistance on the test package is kept below 10^{-3} G's of deceleration by allowing the test package to fall within the 300-pound drag shield. Both drag shield and test package fall together during the drop. The relative positions of the test package and drag shield are shown in Figure 12. The ratio of weight-to-air-drag is kept high so that the deviation from a true free fall will be kept to a minimum. The drag shield is shown in Figure 13.

At impact of the drag shield with the honeycomb paper, air resistance has slowed the drag shield to the point where the test package is approximately 1/2 inch from the bottom of the drag shield. This condition presents no problem since a 3-inch layer of honeycomb paper forms the drag shield floor and gives additional protection to the test package.

When the above technique is used, maximum utilization of available shaft height is obtained. The total shaft height is 62.5 feet and produces 1.85 seconds of weightlessness.

TABLE 1

LOW-GRAVITY SIMULATION METHODS

Method	Zero-Gravity Duration	Size and Dynamics	Remarks
Drop test	1 to 6 seconds	Size limited by tower available: ideal steady transient conditions from 1 G to zero gravity. Impact shock must be controlled.	Comparatively inexpensive, high usage rate, low manpower requirements.
Helicopter drop test	1 to 7 seconds	Unstable conditions prior to true zero gravity. Size limited. Completely self-contained capsule required. Technique has not been demonstrated.	Expensive. High manpower. Scheduling difficult because of aircraft, weather and availability of recovery area. Only one drop per mission.
Aircraft parabolic trajectory	C-131B and KC-135, 15 and 30 seconds trajectory times, 4 to 8 seconds of stabilized zero-gravity time.	Free floating capsule weight limited to approx. 200 lbs. Highly unstable conditions prior to true zero gravity. Test period resulting from oscillations of aircraft. Larger tie down experiments possible. Size limited only by aircraft door.	Expensive. High manpower requirements. Scheduling difficult because of aircraft and weather problems. Comparatively low usage rate.
Missile or rocket	5 to 20 minutes	Size limited. High launch acceleration. Difficult control of tumbling.	Recovery or telemetry necessary. Expensive.
Magnetic or electric field or vibration simulator	Steady state. Zero gravity produced only in very small volume.	Limited size and limited to only paramagnetic materials. Limited heat transfer studies. Technique has not been demonstrated.	High initial cost for equipment. Instrumentation and recording of data difficult because of the high magnetic field.

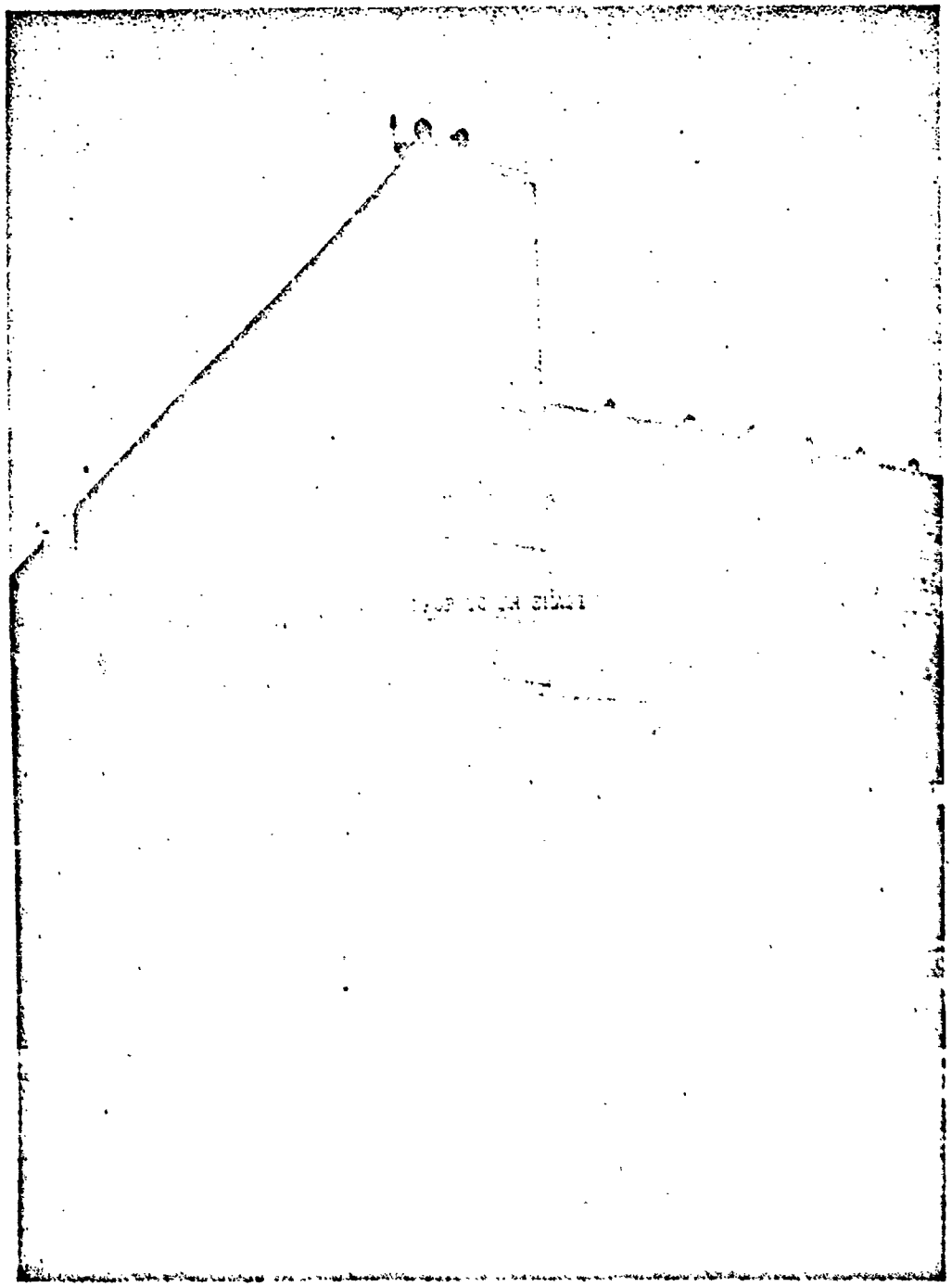

Figure 10. Zero-Gravity Drop-Test Facility

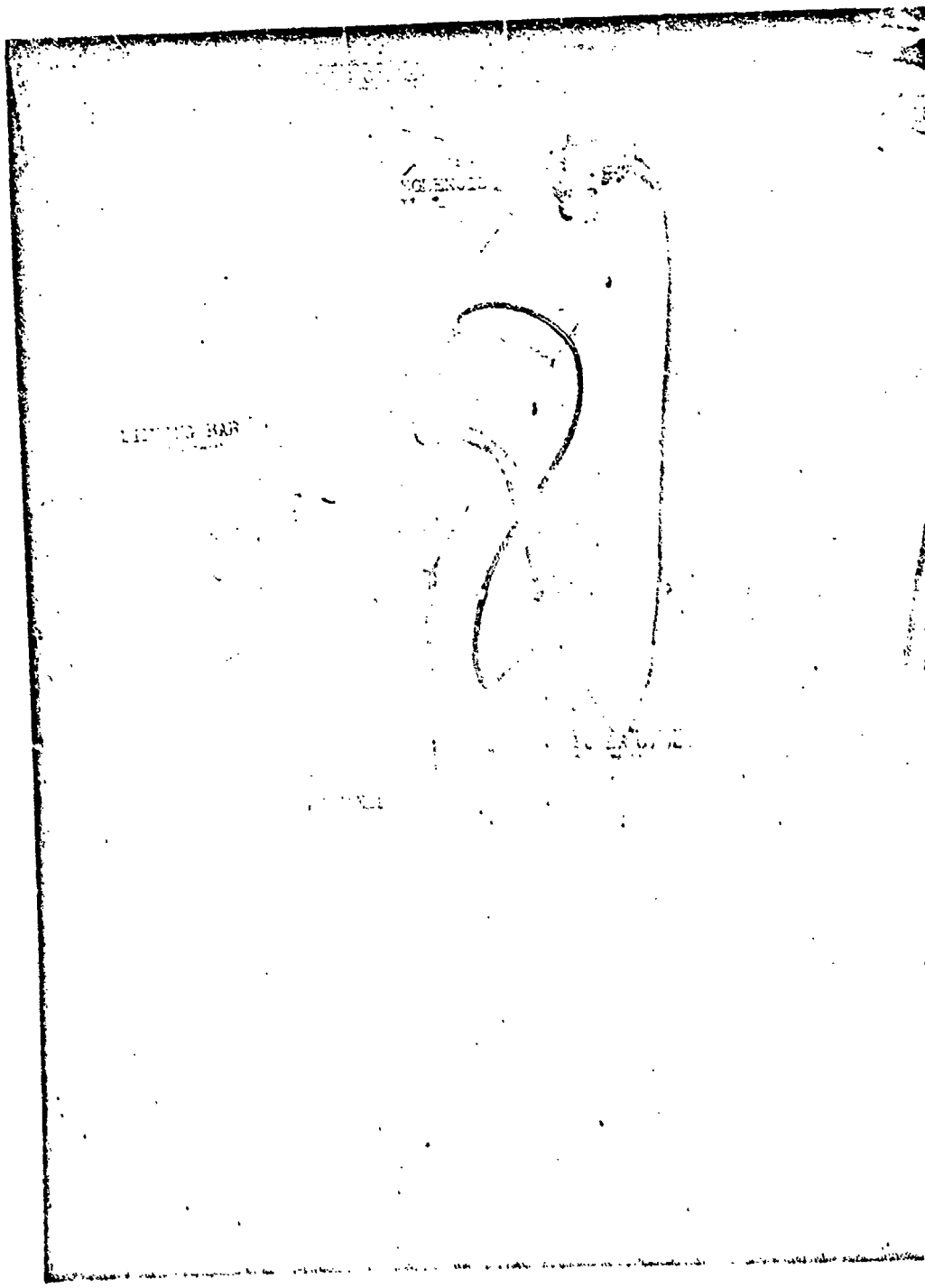

Figure 11. Drag Shield and Honeycomb Paper

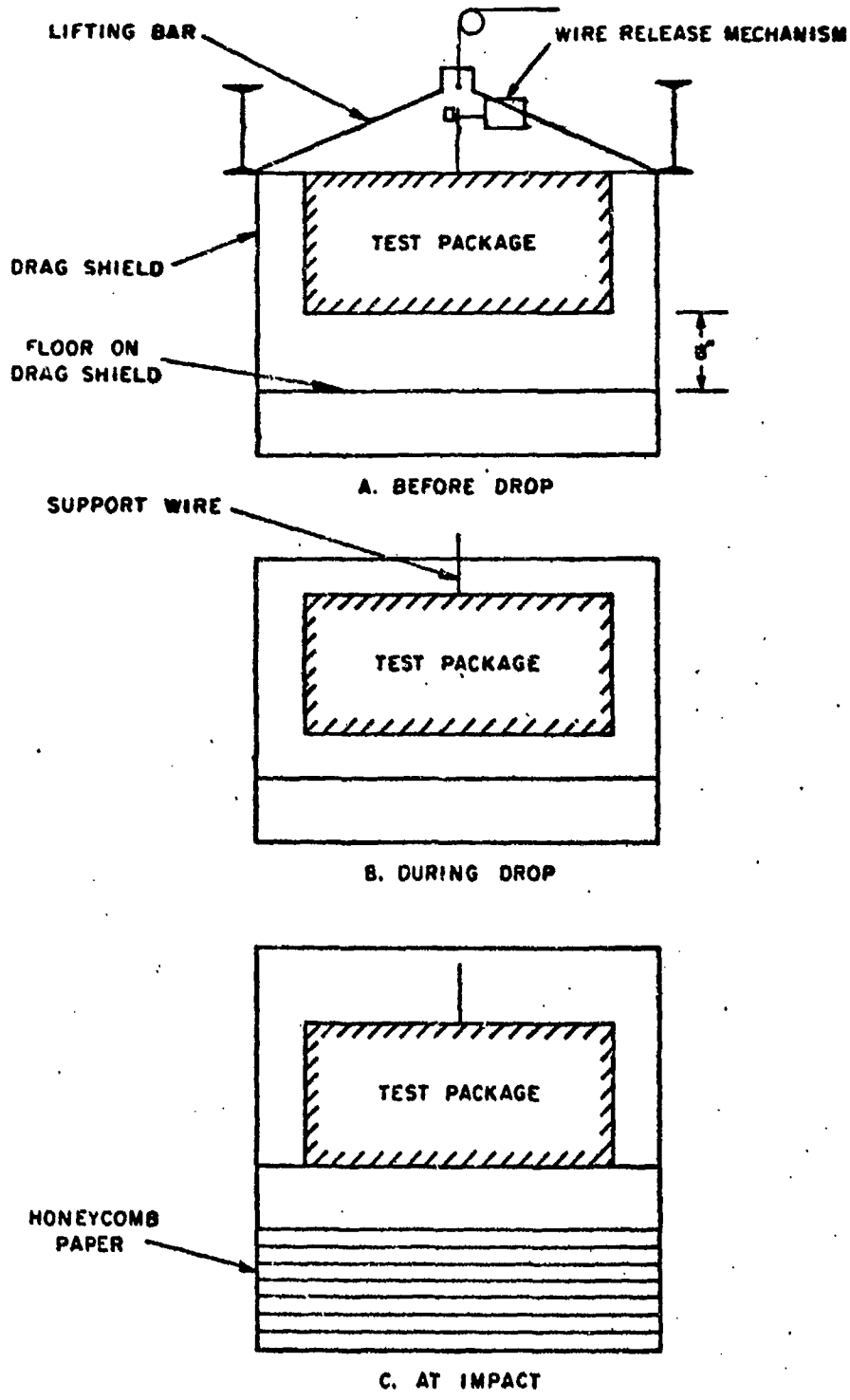

Figure 12. Relative Position of Test Package and Drag Shield

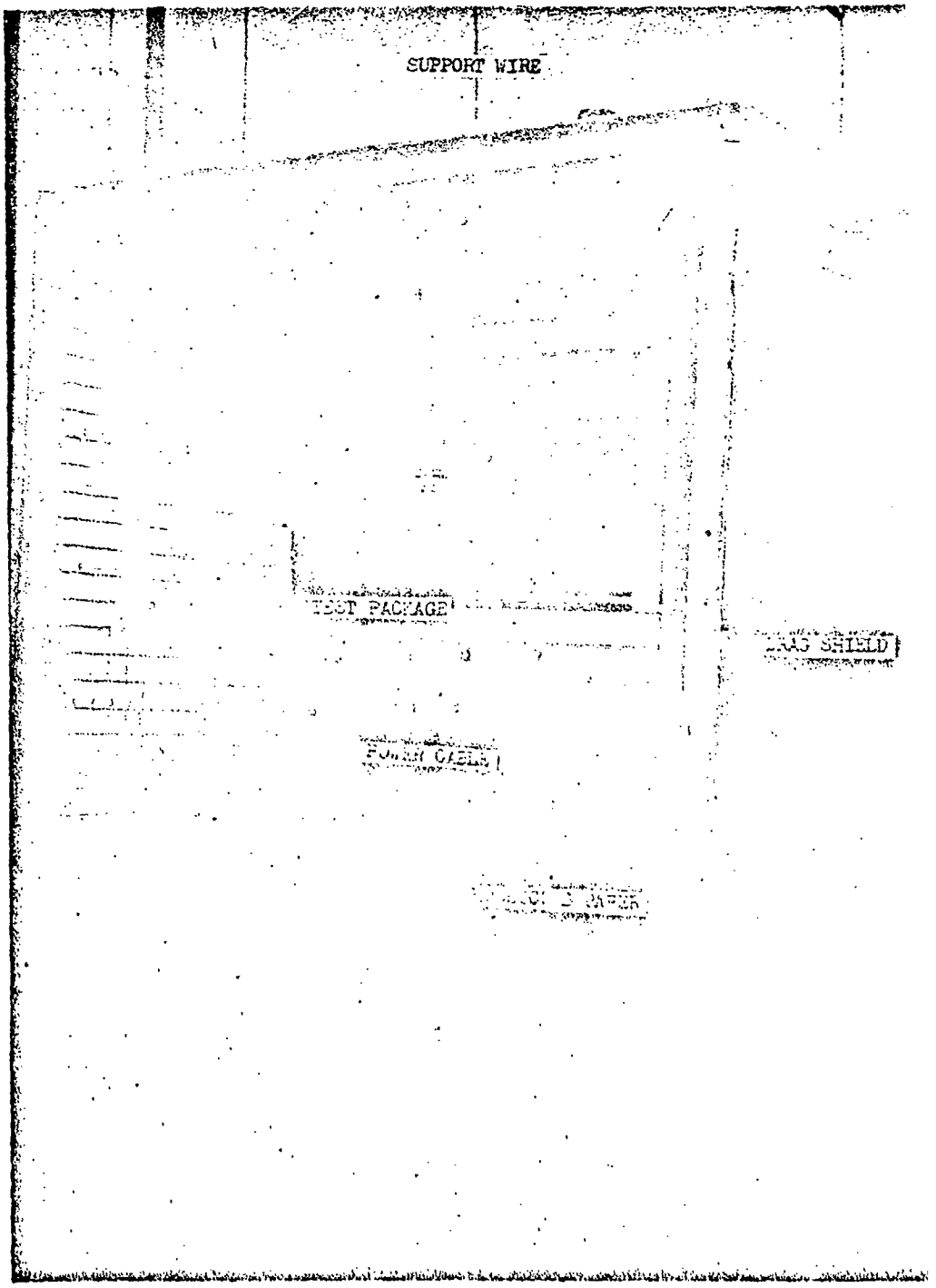

Figure 13. Drag Shield and Test Package

DROP TEST PROCEDURES

The test fluids were contained in Pyrex flasks of various sizes and shapes. These containers were suitably mounted in the test package and illuminated to allow a high-speed motion picture camera to photograph the entire container during free fall. The test package is shown in Figure 14. A 16-millimeter, high-speed, Bell and Howell camera with a 200-foot film capacity was used to obtain the photographic data. The average film speed was 200 frames per second. Illumination of the containers was provided by four 75-watt, 24-volt light bulbs. The containers were mounted inside a light box having a dull white interior finish to keep highlights and glare to a minimum. The light bulbs were arranged to provide indirect lighting. Electrical power for the lights and camera was carried by trailing wires first to the drag shield and then from the drag shield to the test package. These were very light and flexible wires and had no effect on the experiments. Several drops were made with the electrical power supplied from a battery pack mounted in the test package to check the effect the wires had on the experiments. No detectable effect was indicated for identical experiments using the two methods of supplying electrical power.

The liquids used in this investigation were 190-proof ethyl alcohol, triple distilled mercury, distilled water, and chemically pure carbon tetrachloride. The bulk of the experimental data was obtained with wetting fluids, that is, ethyl alcohol and carbon tetrachloride. Mercury represented a nonwetting liquid. We found that distilled water did not give repetitive results and, therefore, was discarded. The properties of these liquids are given in Table 2. Air in every case was in the ullage space above the liquid. The experimental investigations were conducted at essentially ambient pressure and temperature. The contact angle of fluid against Pyrex glass was determined by both the tilting plate and the capillary-rise surface-tension methods. The ring method was used to determine surface tension. The tilting plate apparatus is described in detail in Reference 26.

Before each drop test, the containers were carefully cleaned with a detergent solution in an ultra sonic cleaner and then with chromic acid solution; then rinsed in tap water, then in distilled water, and finally dried with hot air. After cleaning, the containers were filled to the proper amount with the test liquid.

During the initial checkout of the drop facility, an accelerometer was mounted on the drag shield. Using the data obtained on 10 of these initial drops, we determined the free-fall time to be 1.85 seconds. Using this time and counting the film frames from release to impact, we determined an average camera speed for each drop test. On some of the drops, a timing trace using 60-cycle-per-second line current was made by the camera on the film as a check on the preceding method. Any time interval after release of the test package was known to an accuracy of 1.3 percent of that interval.

After the experiment was mounted in the test package, the capsule was balanced and camera operation and alignment were checked. The support wire was attached to the test package and guided through a hole in the top of the drag shield. The wire was then attached to the lifting bar to form a rigid assembly of test package, drag shield, and lifting bar as shown in Figures 11 and 13. The wire was 316 stainless steel and 0.06 inch in diameter. The release mechanism was permanently mounted on the lifting bar and consisted of a double-acting solenoid with a hard steel-knife edge. Actuation of the solenoid forced the knife edge to cut the wire against an anvil, thereby ensuring a smooth release. After the test package was mounted, the hoist at the top of the shaft was energized to lift the entire assembly approximately 3 feet. The honeycomb paper was then placed in position. The paper was a glued assembly of 13 layers of honeycomb 19 inches by 26 inches in cross section and 39 inches in height.

From this point on, the drop operation was conducted from the control room. The capsule assembly was then hoisted to within 2 inches of the I-beam supports at the top of the shaft. Final positioning of the lifting bar against the I-beam supports was accomplished by a motor-driven actuator that deflected the hoisting cable. See Figures 15 and 16. This positioning made a completely rigid assembly at the top of the shaft. After about 10 minutes, the camera and lights were energized; then after 10 seconds, the wire release mechanism was energized cutting the support wire and releasing simultaneously both the test package and drag shield.

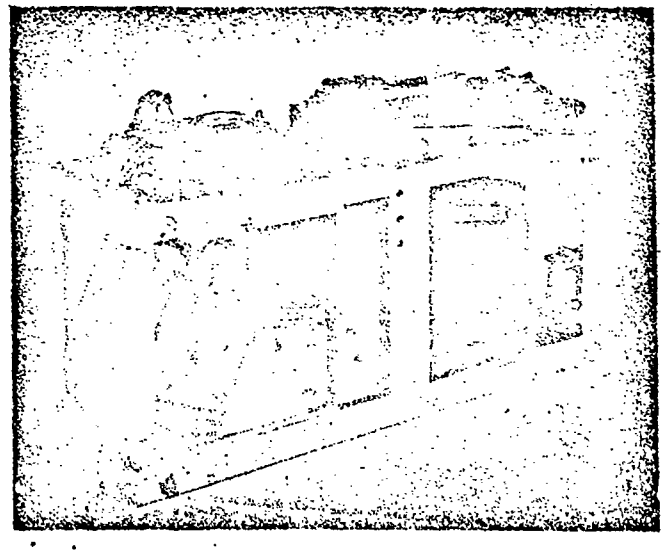

Figure 14. Test Package

TABLE 2

TEST FLUID PROPERTIES

Fluids	Density (grams per cm^3 at 20°C)	Viscosity (centipoises at 20°C)	Surface Tension in Air at 20°C ($\frac{dynes}{cm}$)	$\frac{\text{Surface Tension}}{\text{Density}}$ ($\frac{cm^3}{sec^2}$)	Contact Angle with Pyrex (deg)
Mercury	13.55	1.554	476	35.1	120-125
Ethyl Alcohol	0.7893	1.200	22.3	28.3	20-26
Carbon Tetra-chloride	1.595	0.969	26.95	16.9	16-19
Distilled Water	0.9982	1.005	72.8	73	less than 12

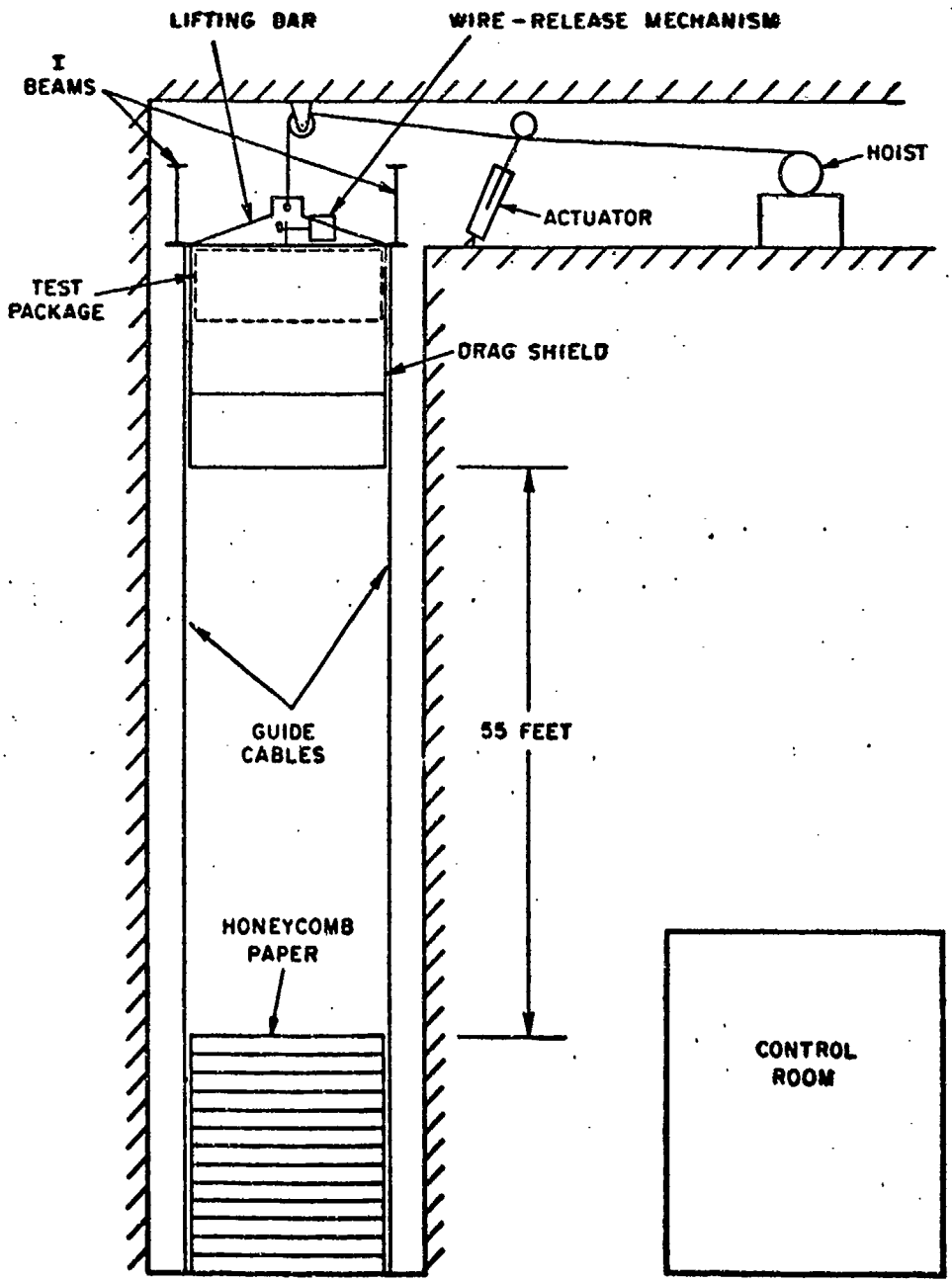

Figure 15. Schematic of 1.8-Second Drop Facility

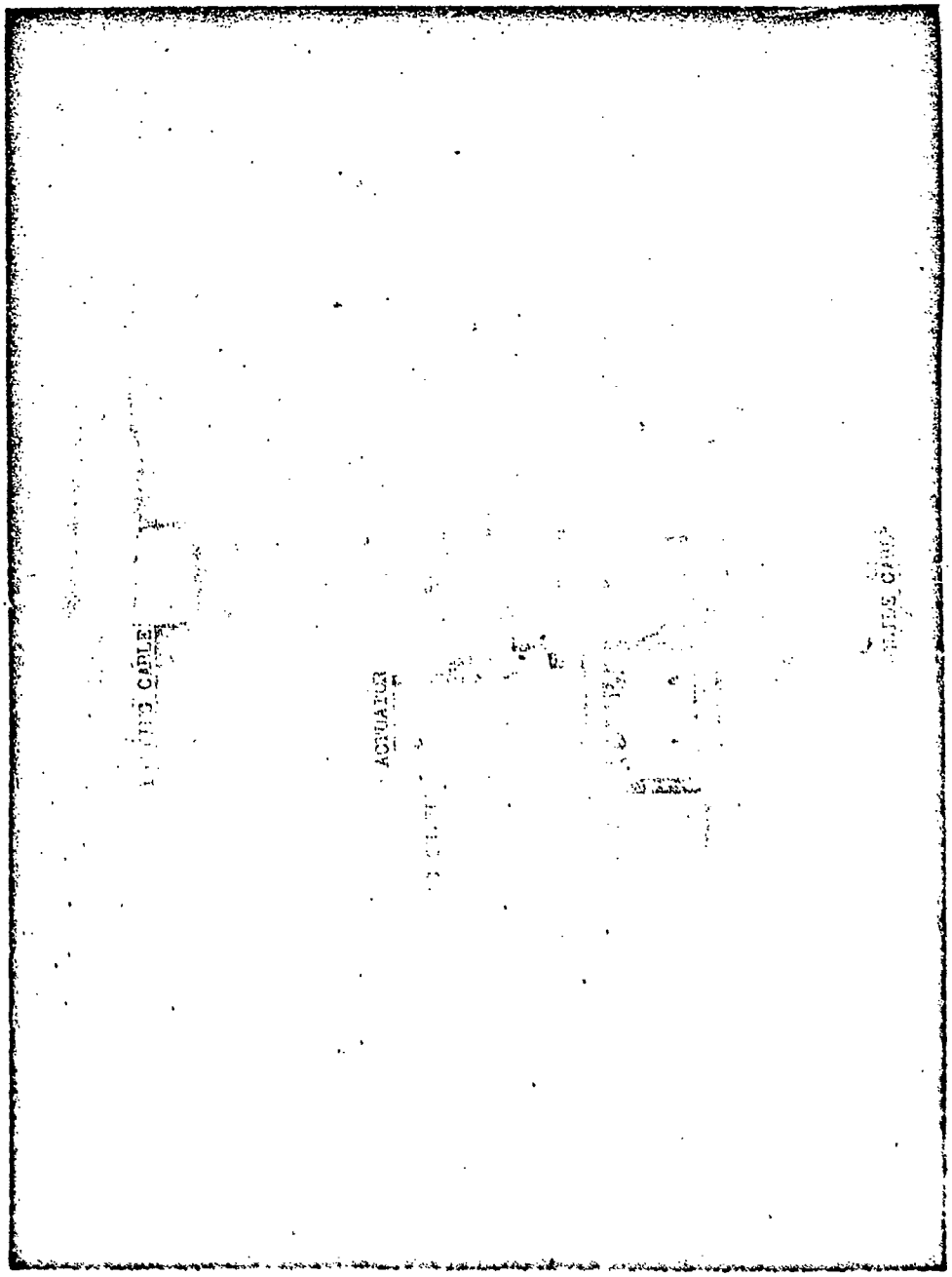

Figure 16. Final Positioning of Drop Capsules

STATIC FLUID CONFIGURATIONS IN CYLINDRICAL CONTAINERS

Since the contact angle (θ) is known to be preserved at zero gravity and since the minimum energy principle requires a liquid-vapor interface of constant curvature, which for an unrestricted cylinder would be a section of a sphere, the zero-gravity configuration may be determined. Figures 19 and 20 give the displacement of the interface for the entire range of contact angles. These figures assume no end effects or restriction in the container. Also a gradual translation from positive to zero gravity is assumed. These predictions were verified in the drop tower for fluids of zero contact angle. Figure 21 illustrates both the 1-G and zero-G configuration for ethyl alcohol. Identical results were obtained with carbon tetrachloride and distilled water. A point was also verified for the nonwetting fluid configuration using mercury. In all cases in these experiments, there was an overshoot of the equilibrium position during the formation process. This condition will be discussed in detail later on. The percent of liquid and diameter-to-length ratio (D/L) of the cylinder container also has an effect on the static interface configuration. Figure 22 gives this effect for wetting fluids and Figure 23 deals with nonwetting fluids. Figure 17 illustrates the use of Figures 22 and 23.

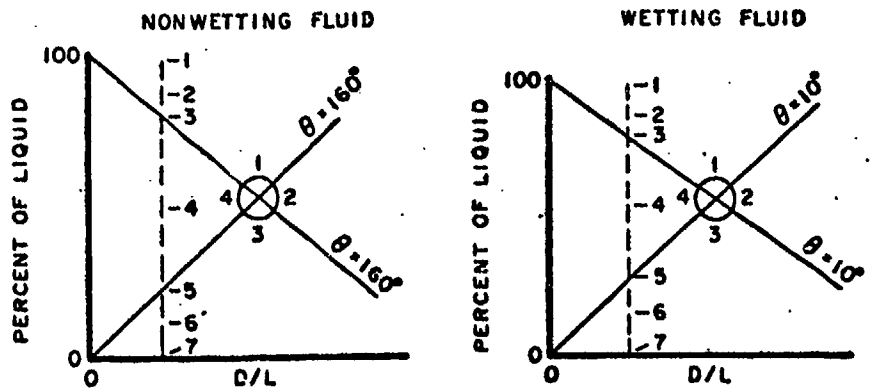

Figure 17. Use of Wetting and Nonwetting Fluid Configurations in Cylindrical Tanks

For a given container (D/L constant) and fluid (θ constant), the configuration is as shown in Figure 18.

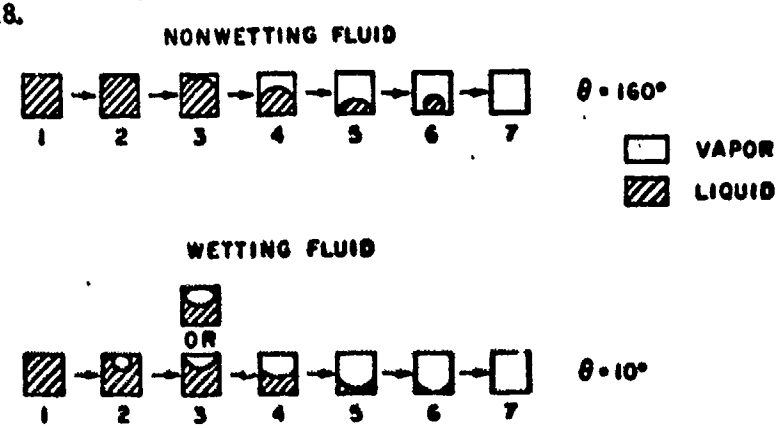

Figure 18. Progression of Wetting and Nonwetting Fluids for Drain Operation Under Zero-Gravity Conditions

In Figures 22 and 23, the common point of the four-configuration regions is an unstable configuration. For a fill operation under zero-gravity condition with nonwetting fluids, the progression of fluid configurations can be determined from the appropriate figure. However, in going from configuration region 3 to 4, a vapor volume may be trapped at the fill end of the container.

Note that for a drain operation involving wetting fluids under zero-gravity conditions, which proceeds from configuration region 1 to region 4, some liquid may be trapped at the vapor end of the container. For $\theta = 0°$, the vapor bubble of configuration region 1 is not restricted to the position shown and may be found any place in the bulk liquid. If a θ of 180° is possible, the liquid bubble of configuration region 3 may "float" off the walls of the container.

From this discussion, we may conclude that Figures 20 and 21 on interface displacement apply only for D/L and percent of liquid combination lying in configuration region 4 of Figures 22 and 23.

Several drop tests were performed using ethyl alcohol in a Pyrex cylinder (D/L = 1.4) to determine the effect of initial fluid position on final interface configuration. Figure 24 gives both the 1-G and zero-G configuration with the axis of the cylinder vertical. Referring to Figure 22 with $\theta = 0$, D/L = 1.4, and 50 percent liquid, we determined that both configuration regions 1 and 4 were possible and the zero-G configuration, therefore, verified. Figure 25 gives configurations for ethyl alcohol (25 percent) with the cylinder axis horizontal and at a 45-degree angle. By checking Figure 22 for these conditions, one can predict both configuration regions 4 and 3. The test results check with the predictions; however, when the axis of the cylinder was horizontal, the fluid was located at both ends of the containers or a "double" configuration 3. This condition resulted because the initial probability for locating at either end of the cylinder was the same. The experiment was repeated with the 75-percent fill. Prediction of configuration region 1 is shown in Figure 22. The results were as predicted as shown in Figure 26.

Experiments were also conducted in the KC-135 and C-131 aircraft. The procedures for aircraft testing are given in Reference 25. Since the aircraft provides long periods of zero gravity, larger containers could be investigated. The fluids considered were H_2O, carbon tetrachloride, ethyl alcohol, and mercury. The cylinders were approximately 5, 10, and 15 centimeters in diameter. The configuration obtained was similar to the drop-tower results as illustrated in Figures 27 through 29. Since in aircraft testing, the positive to zero-gravity translation does vary from run to run, this condition was found to produce two different stable configurations as shown in Figure 27. This fact points out that if a designer is to utilize the minimum energy principle to control fluid orientation, an accurate knowledge of the effect of the G translation is necessary. As the size of the cylinder was increased, obtaining the stable zero-gravity configuration became increasingly difficult. The 15-centimeter container illustrated in Figure 29 was the largest cylinder investigated.

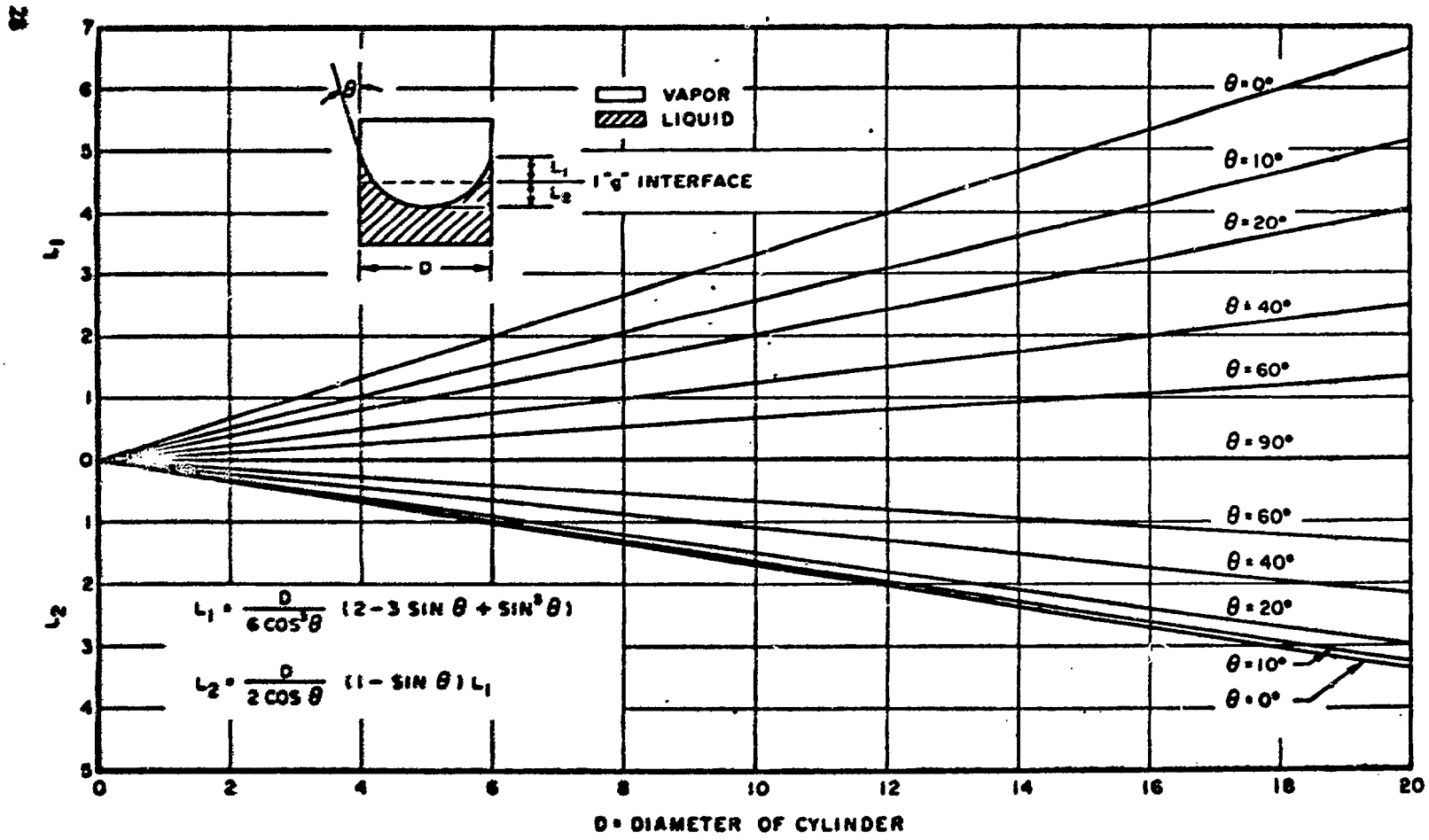

Figure 19. Displacement of Wetting Fluid Interface in a Cylindrical Tank

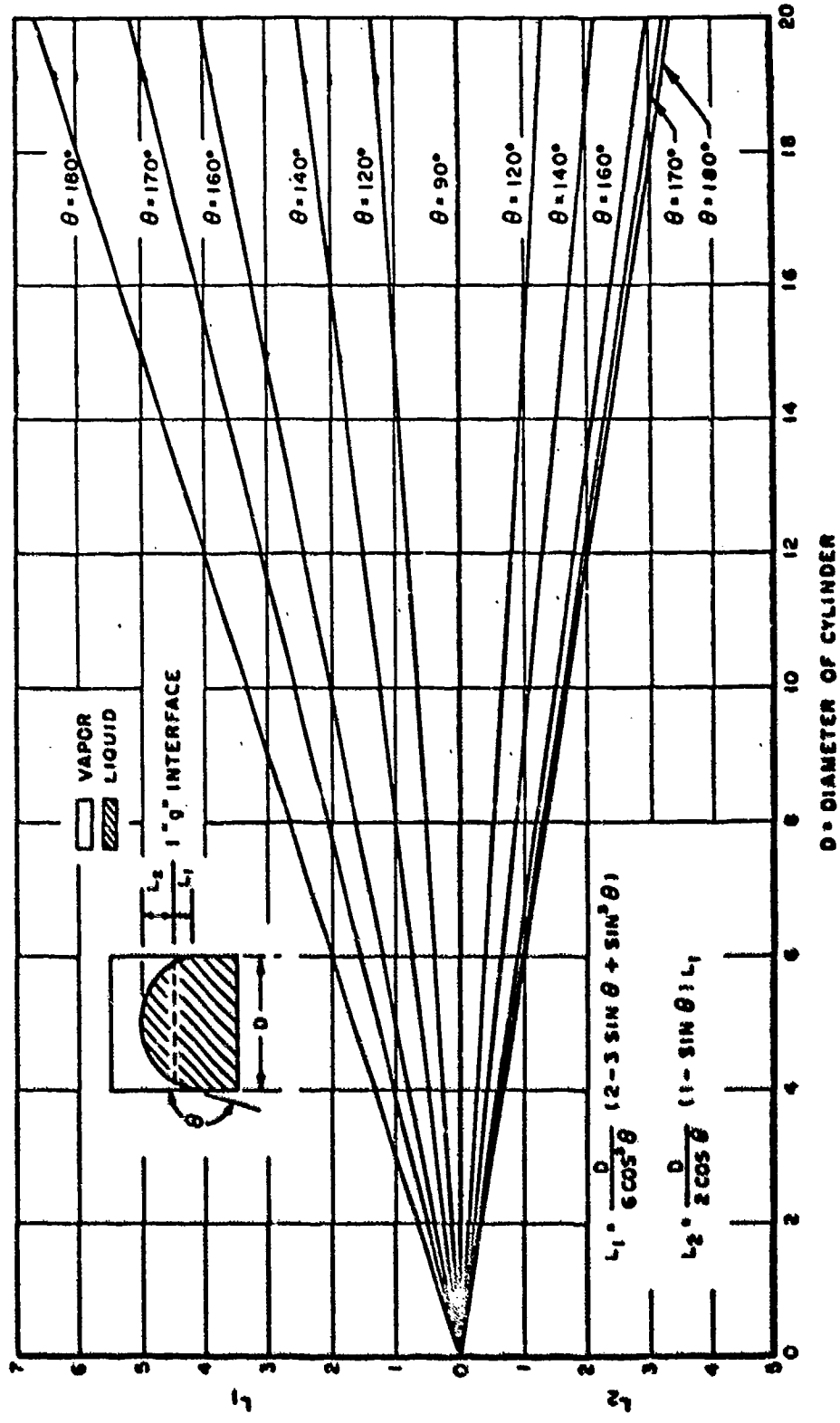

Figure 20. Displacement of Nonwetting Fluid Interface in a Cylindrical Tank

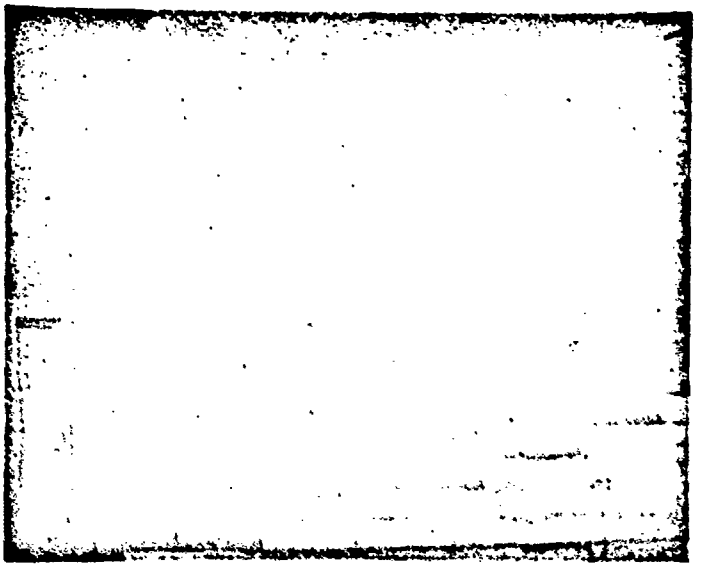

1 G

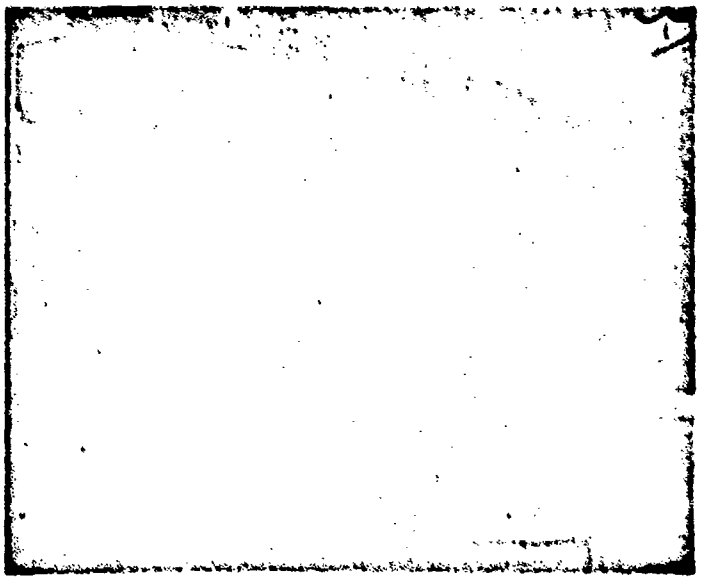

ZERO G

Figure 21. Configurations of Ethyl Alcohol in Cylinders with Inside Diameters of 0.912, 0.825, 0.759, 0.600, 0.575, 0.525, and 0.418 Inches

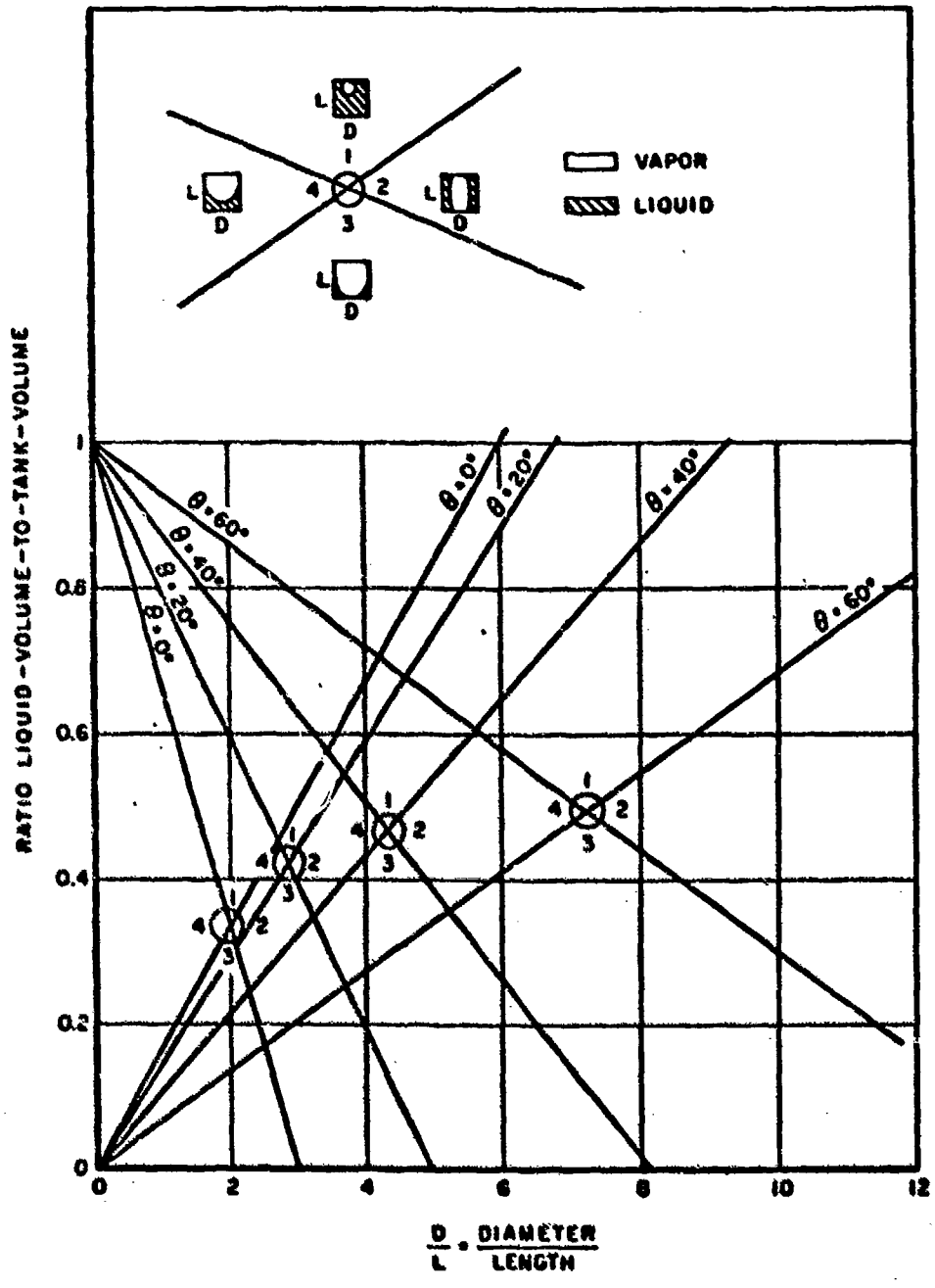

Figure 22. Wetting Fluid Configurations in a Cylindrical Tank

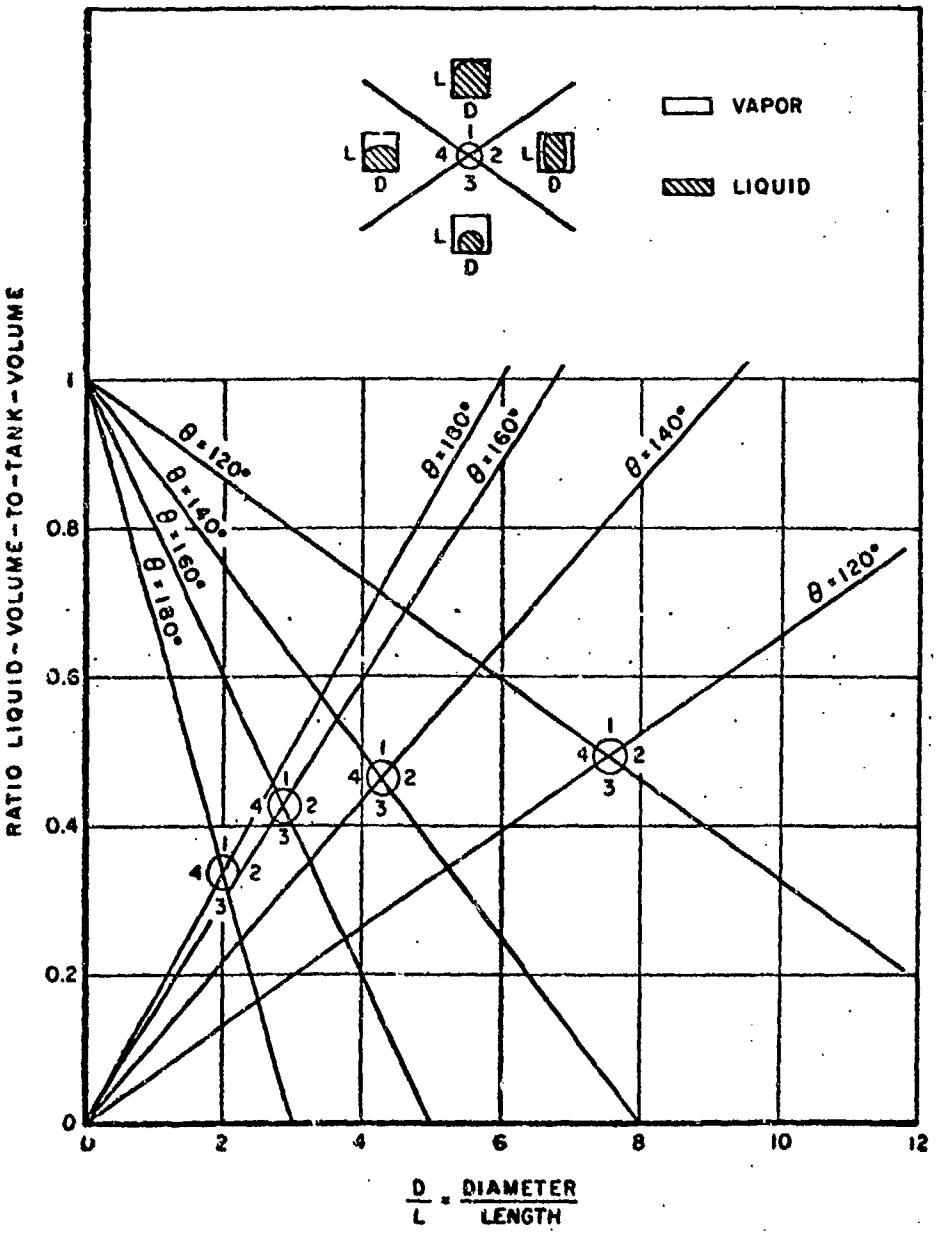

Figure 23. Nonwetting Fluid Configurations in a Cylindrical Tank

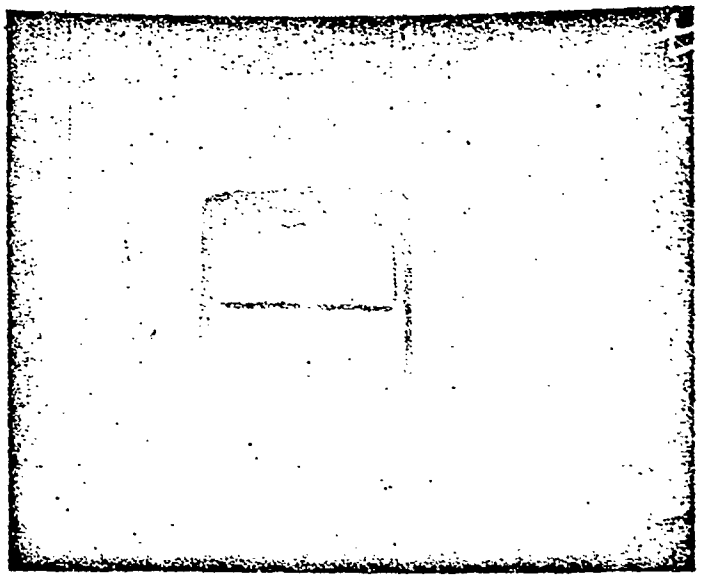

1 G

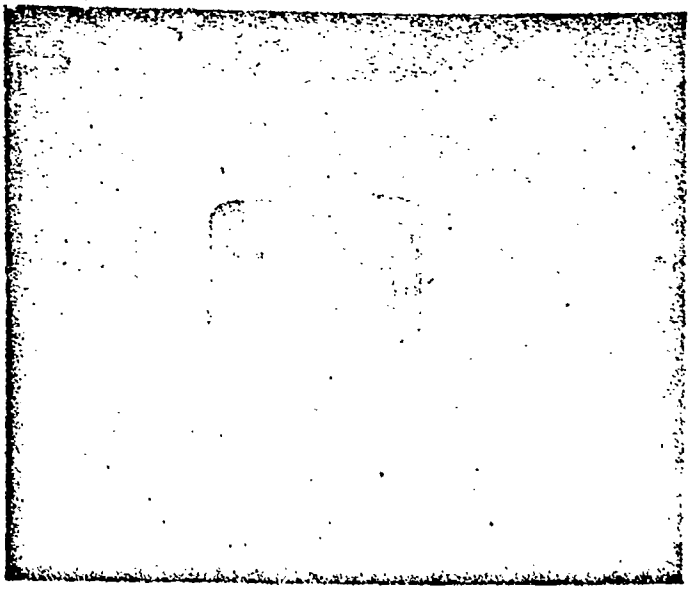

ZERO G

Figure 24. Configurations of Ethyl Alcohol (50 Percent Fill) with Axis of Cylinder (D/L = 1.4) Vertical

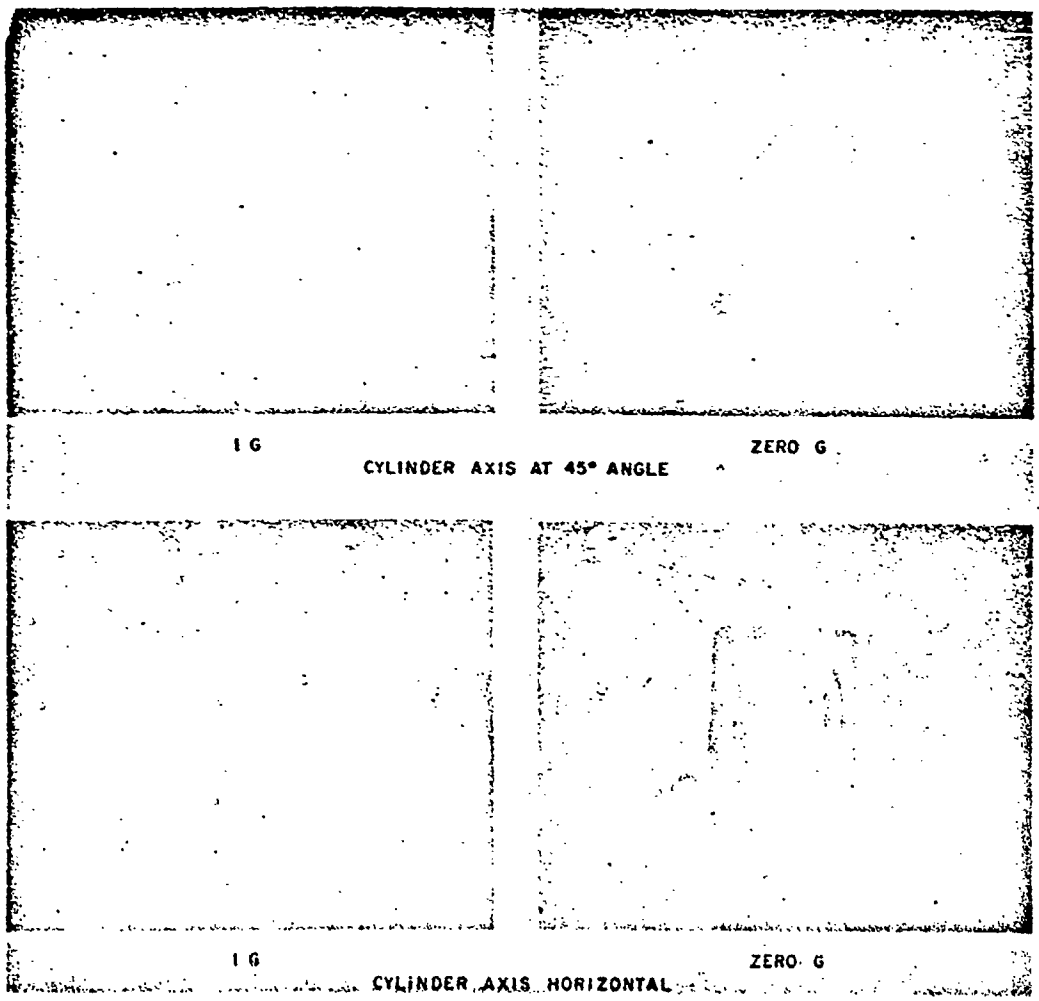

Figure 25. Configurations of Ethyl Alcohol (25 Percent Fill) with Axis of Cylinder ($\Gamma'/L = 1.4$) Horizontal and 45 Degrees

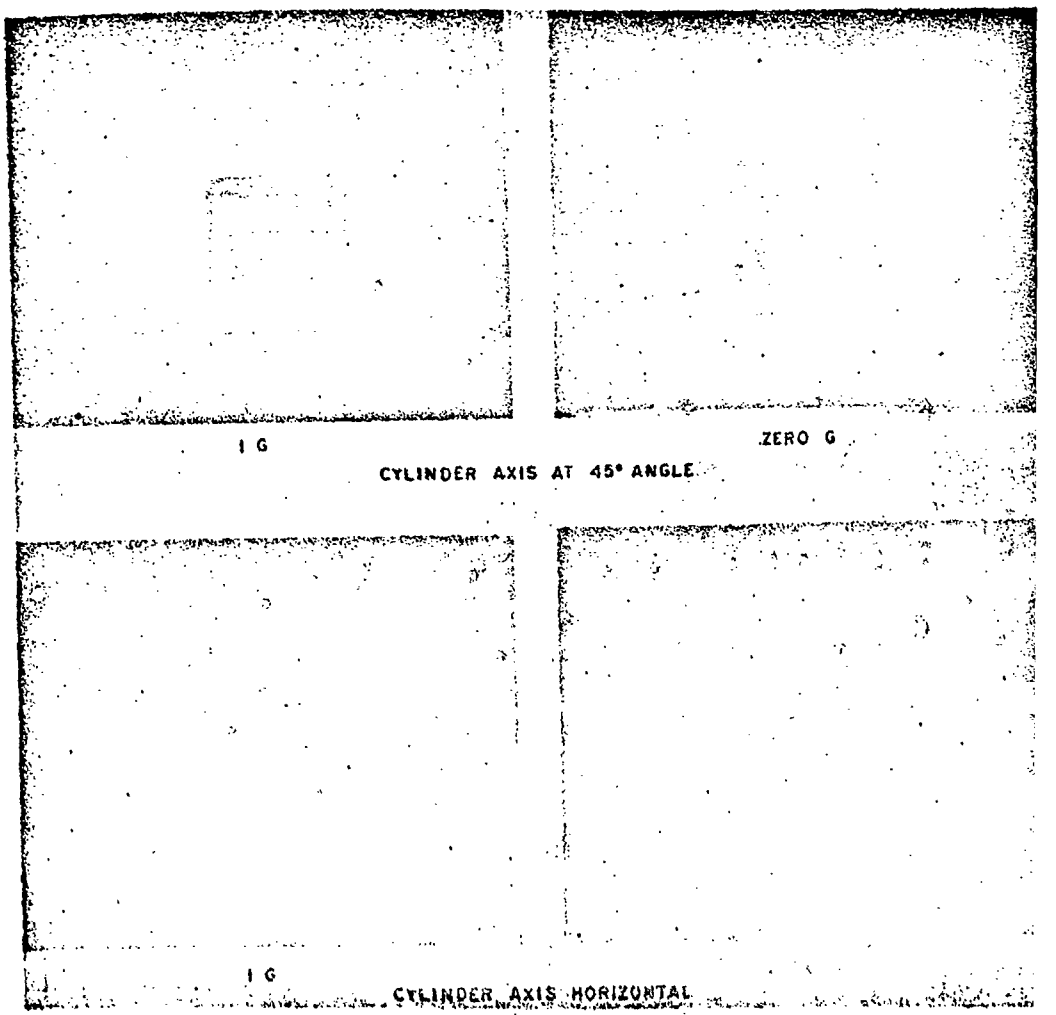

Figure 26. Configurations of Ethyl Alcohol (75 Percent Fill) with Axis of Cylinder (D/L = 1.4) Horizontal and 45 Degrees

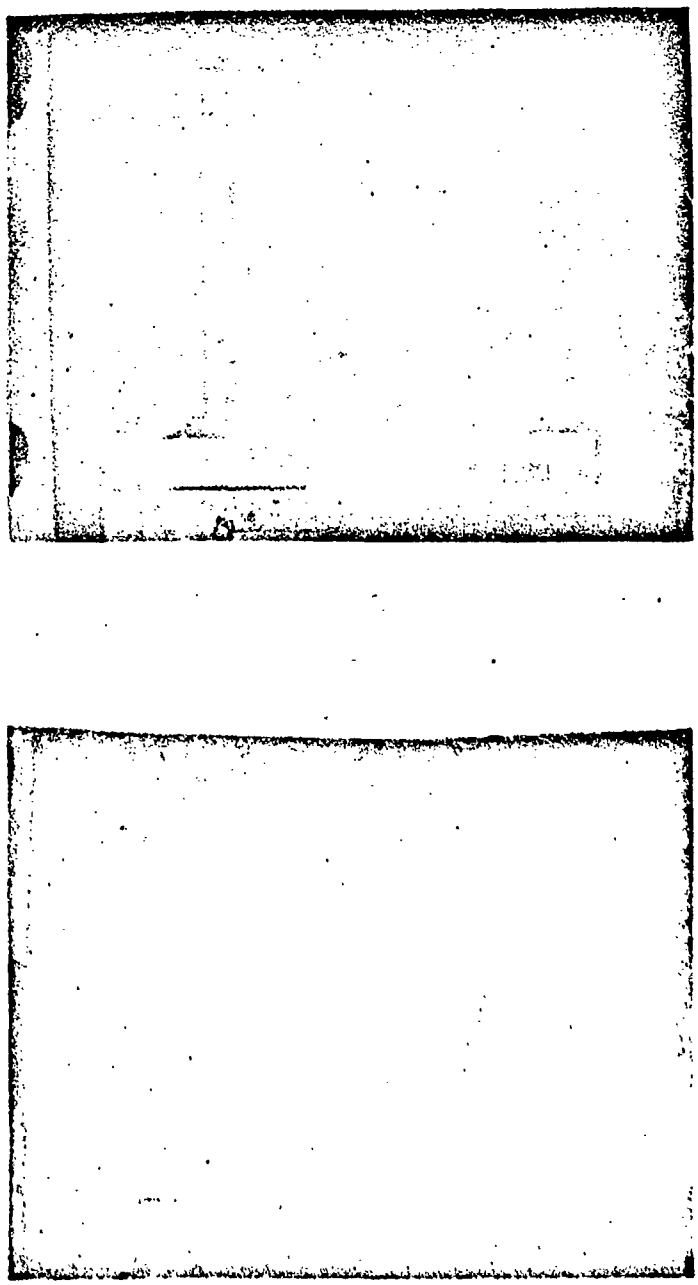

Figure 27. Two Low-Gravity Configurations of Ethyl Alcohol (50 Percent Fill) in 5-Centimeter Inside-Diameter Cylinder (Aircraft Test)

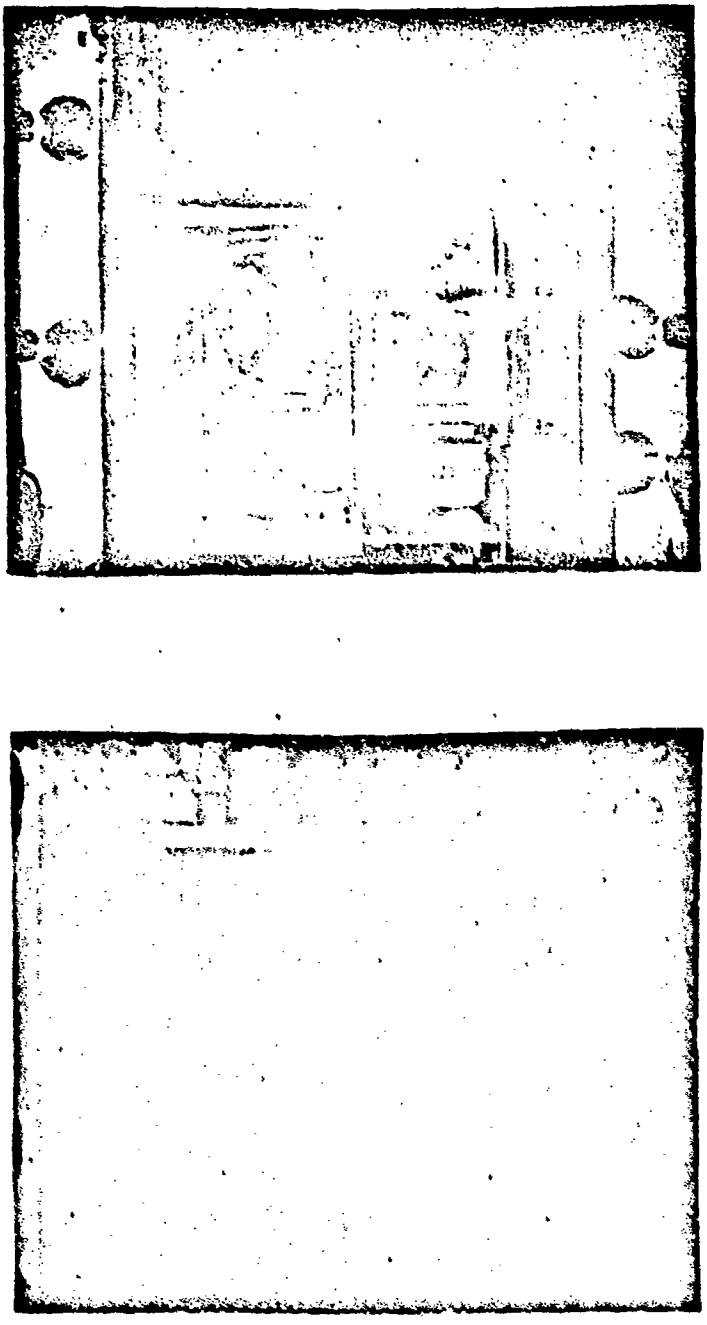

Figure 28. Low-Gravity Configurations of Carbon Tetrachloride and Mercury in 10-Centimeter Inside-Diameter Cylinder (Aircraft Test)

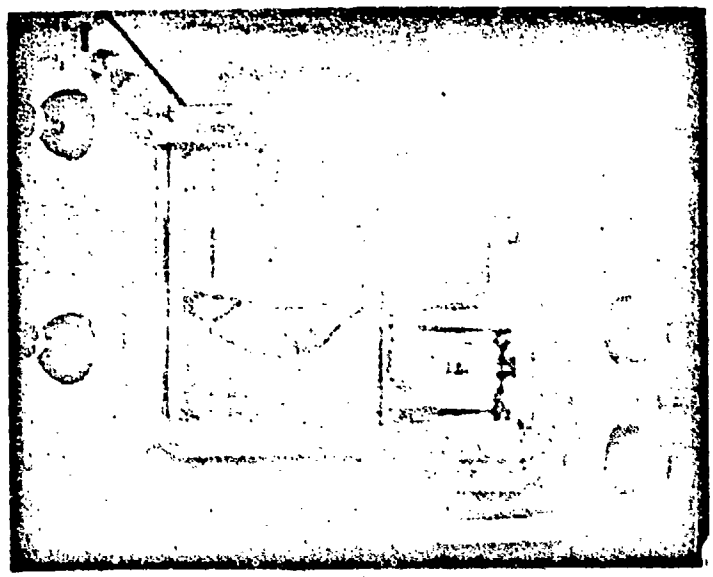

15-cm INSIDE DIAMETER

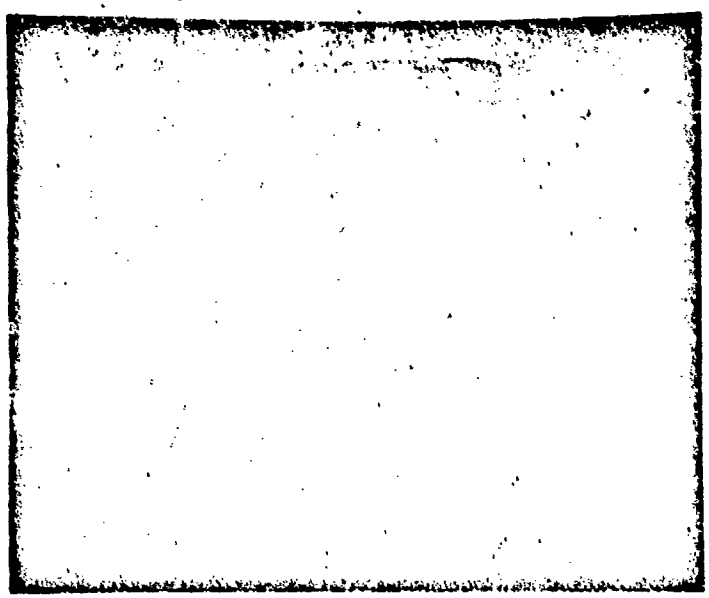

5.5-cm INSIDE DIAMETER

Figure 29. Low-Gravity Configurations of H_2O (50 Percent Fill) in 15-Centimeter Inside-Diameter and 5.5-Centimeter Inside-Diameter Cylinders (Aircraft Test)

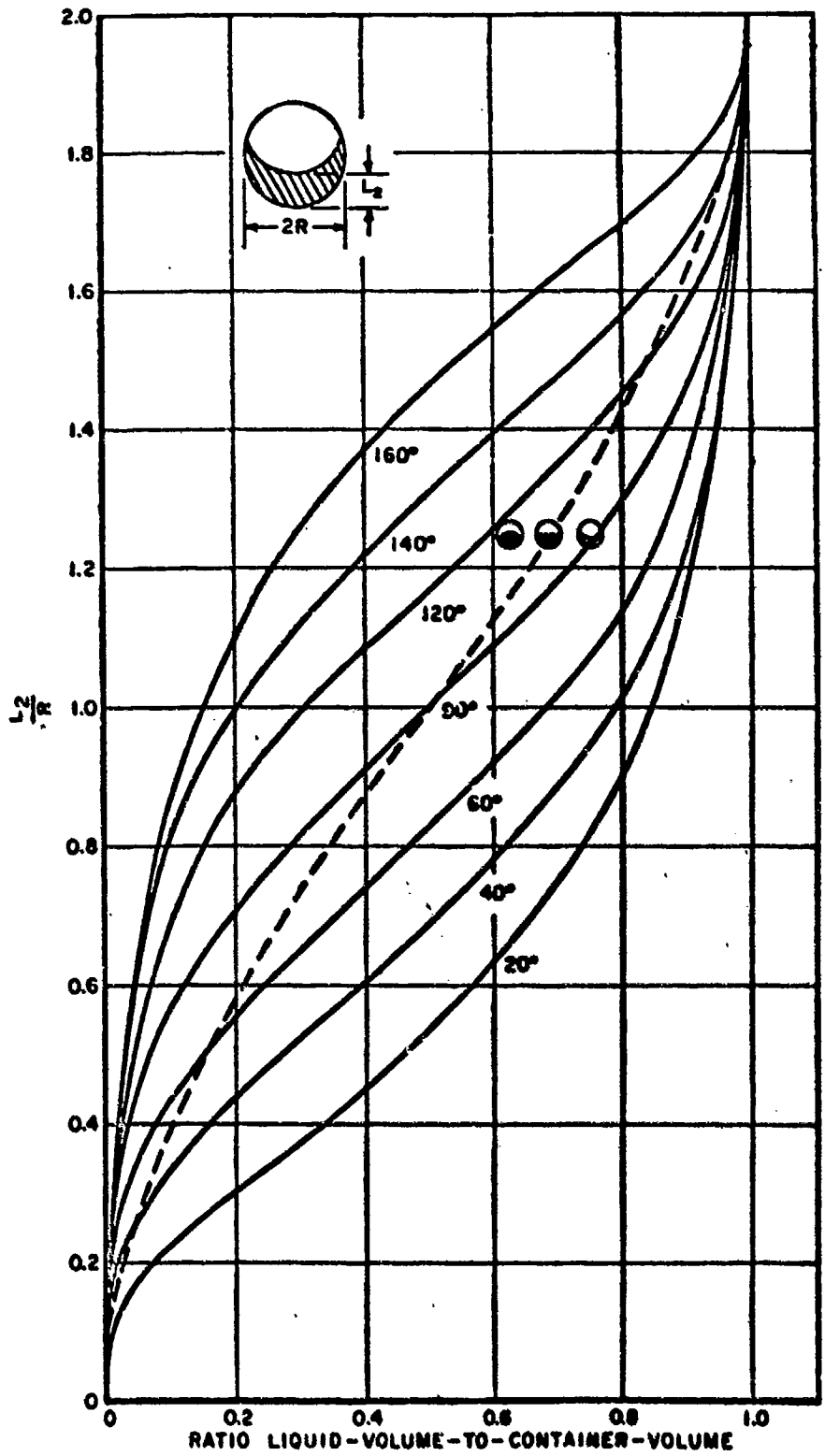

Figure 30. Fluid Configurations in a Spherical Tank (Center of Interface Displacement)

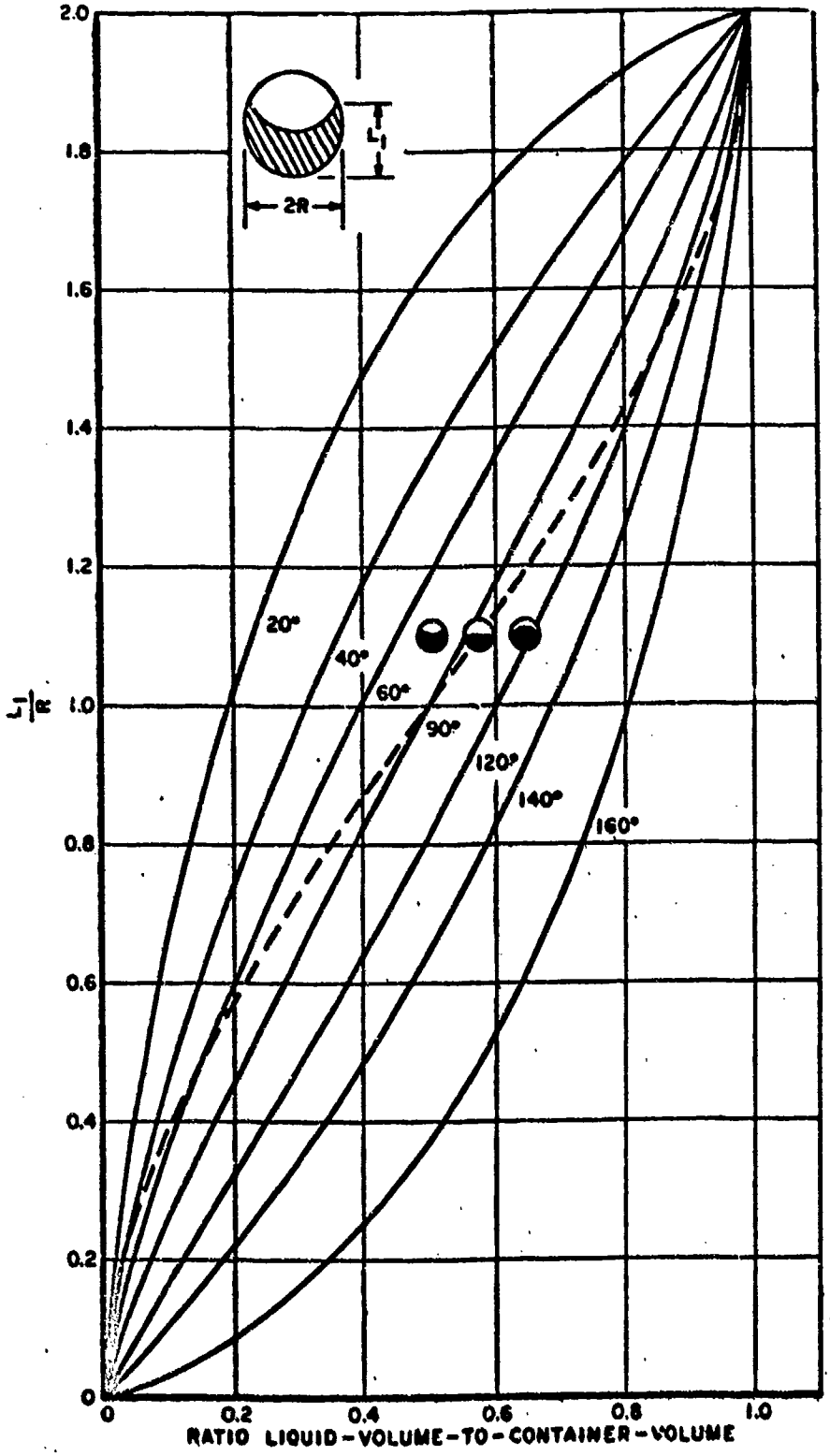

Figure 31. Fluid Configurations in a Spherical Tank (Edge of Interface Displacement)

1 G

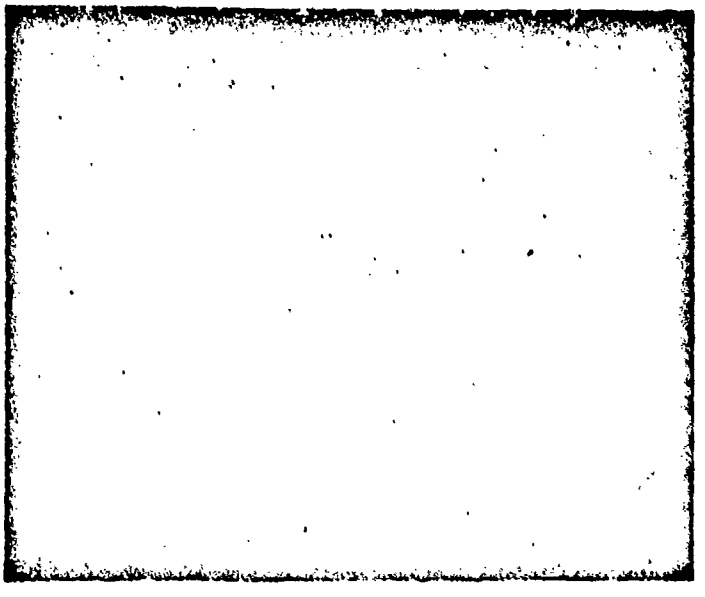

ZERO G

Figure 32. Configurations of Mercury in 100-Milliliter Sphere

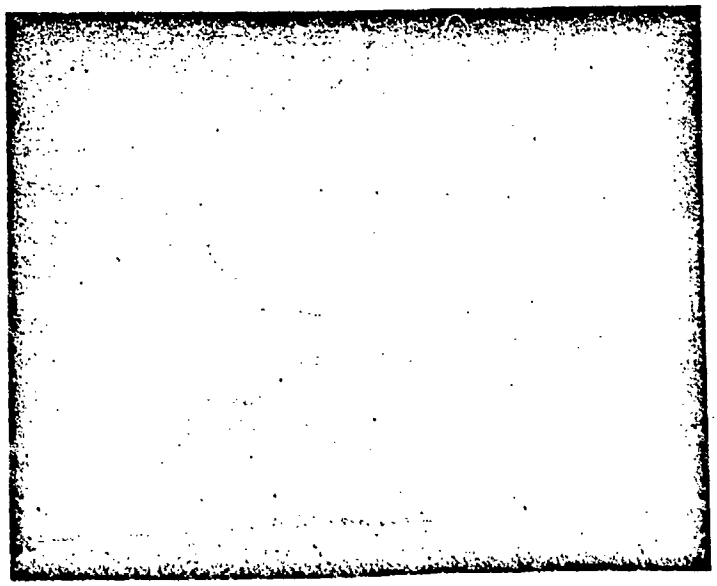

1 G

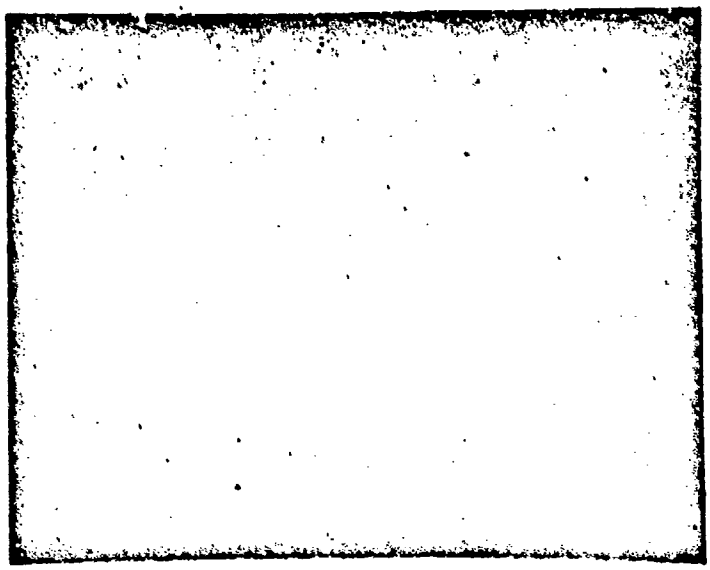

ZERO G

Figure 33. Configurations of Mercury (25 Percent Fill) in 100-Milliliter Sphere

1 G

ZERO G

Figure 34. Configurations of Mercury (25 Percent Fill) in 300-Milliliter Sphere

1 G

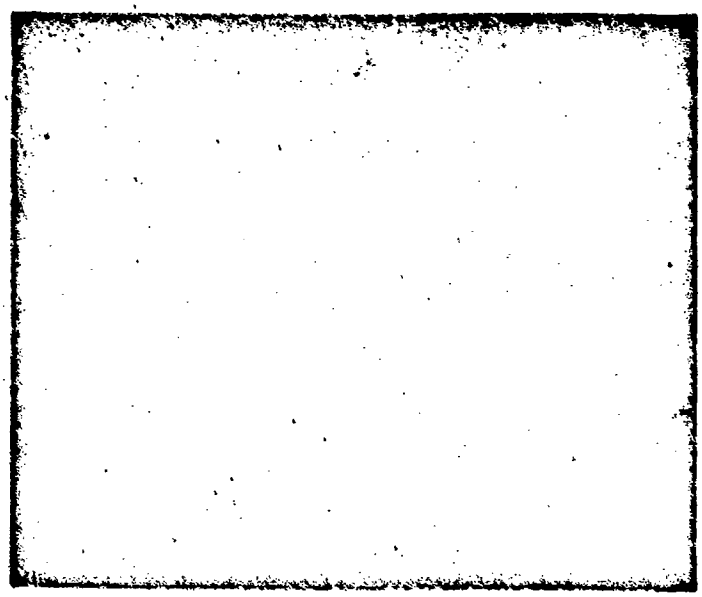

2(6G) G

Figure 35. Configurations of Ethyl Alcohol (50 Percent Fill) in 500-Milliliter Sphere

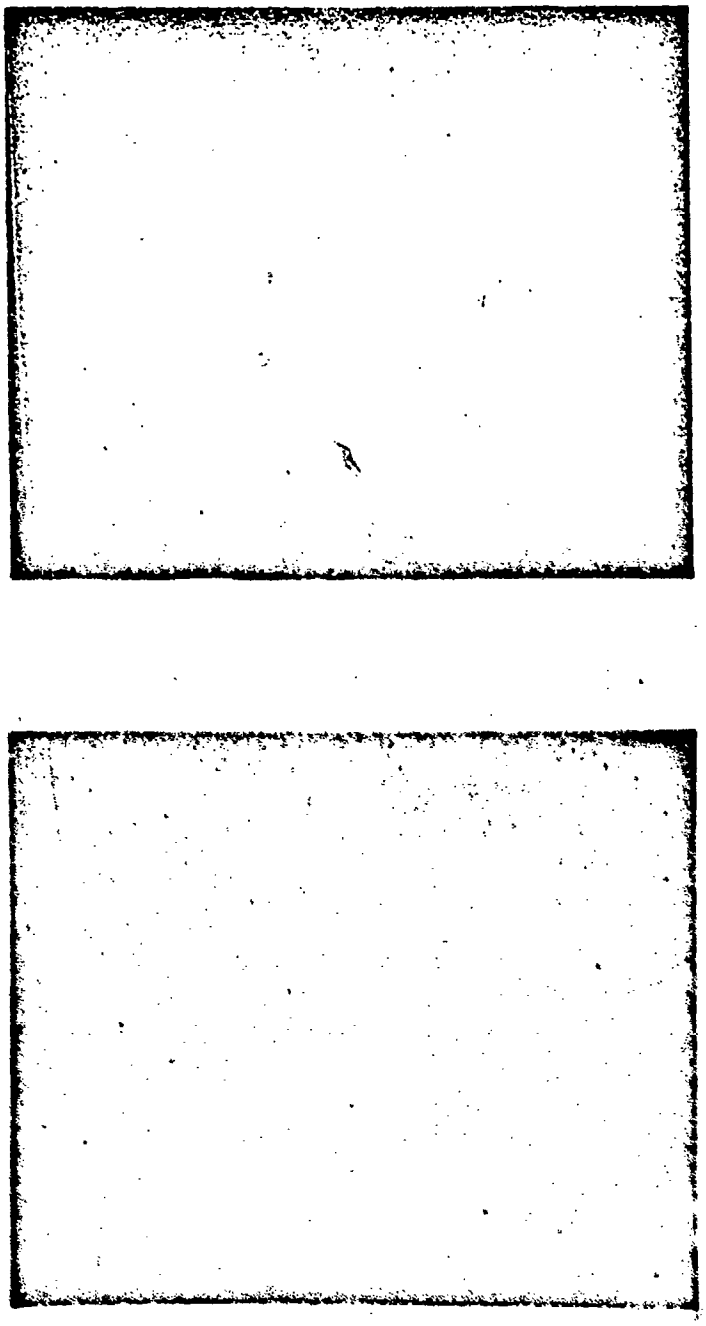

Figure 36. Configurations of Carbon Tetrachloride (50 Percent Fill) in 100-Milliliter Sphere

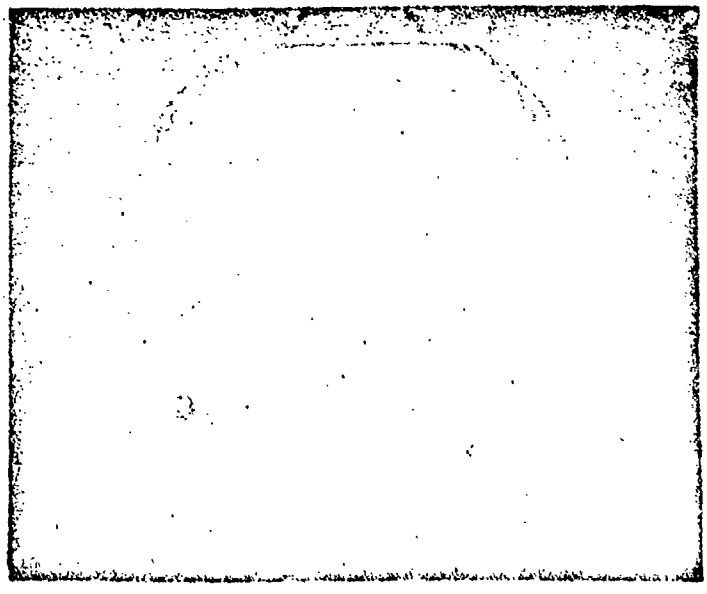

Figure 37. Configurations of Carbon Tetrachloride (50 Percent Fill) in 500-Milliliter Sphere

INTERFACE OVERSHOOT

The displacement of the edge and center of the liquid-vapor interface in a cylinderical container was determined by a frame-by-frame analysis of several drop tests with ethyl alcohol. The results are displayed in Figure 39. Note that there is an "overshot" by the interface of the equilibrium zero-gravity configuration. This overshoot phenomenon may in special cases present problems for the designer of propellant tanks utilizing surface tension for fluid orientation. An example might be the following. Note Figure 22, if the tank was designed so that the translation from positive to zero gravity occurred at a fill ratio only slightly below the line separating configuration regions 1 and 4, the overshoot could cause a translation from region 1 to region 4. Once in region 4, for fluids with contact angles other than zero, the overshoot may cause the vapor bubble that would normally be wall bounded to break free of the wall and "float" internal to the liquid. In most cases the problem of overshoot can be circumvented by proper design. Acceleration perturbations during the translation to low gravity has a more important effect on the low-gravity liquid-vapor configuration. This effect has been noted many times in comparing the results of aircraft tests with results of drop tests. This situation brings out a point that is often omitted when determining low gravity configurations using the minimum energy principle. Depending on the initial condition of the fluid as the low-gravity environment is reached, there are many relative minimum energy states for the fluid. That is, the fluid may stabilize in a relative minimum energy configuration, and the surface energy must be increased to drive the fluid from this "energy well" to the absolute minimum energy configuration. This condition is illustrated in Figure 38.

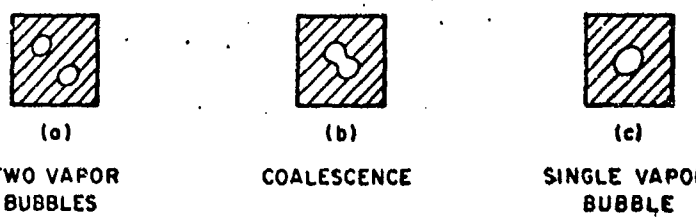

Figure 38. Surface Energy Conditions

Figure 38a shows a condition of relative minimum energy. This condition has been noted many times in aircraft tests at ASD. Figure 38b shows that the condition at coalescence requires a higher energy state because of the increase in liquid-vapor interface area. Coalescence has not been noted in aircraft tests for times as high as 15 seconds. Figure 38c shows a condition that would be predicted by the minimum energy principle.

Using liquid-liquid models (two equal density insoluble fluids), we found that after generating several bubbles (condition 1) approximately 15 minutes were required to obtain condition 3. The coalescence could possibly be explained by the presence of small velocity and/or thermal gradients that could support the coalescence. The rate at which coalescence occurs at low gravity is of extreme importance in some heat-transfer processes.

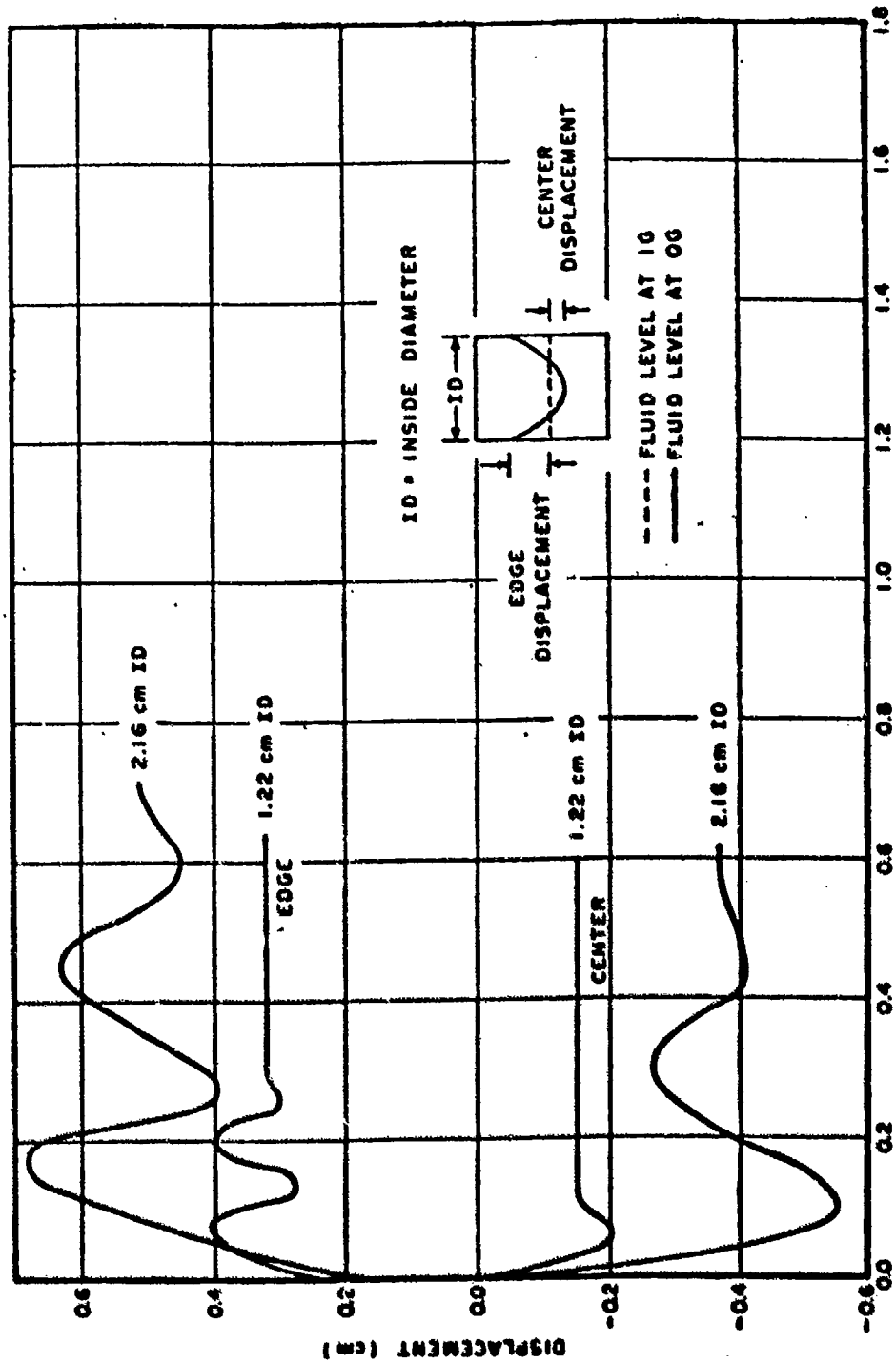

Figure 39. Interface Displacement History for Ethyl Alcohol (50 Percent Fill) in 2.16-Centimeter

CONCLUSIONS AND RECOMMENDATIONS

The following conclusions and recommendations are made:

1. The drop test facility is a useful tool for providing basic information on fluids of low gravity.

2. The absolute minimum energy configuration of fluid at zero gravity in simple container may be readily determined.

3. Depending on the condition of fluids during the transfer from positive to zero gravity and the type container, the fluid may stabilize in a relative minimum energy configuration.

4. All real fluid will eventually form into low-gravity configuration with the liquid phase wall bounded.

5. In the capillary system, screens can be made to act as solid surfaces. This appears to be one method of controlling fluid orientation with low-weight penalty.

6. The momentum associated with the fluid during the transfer from positive to low gravity will cause an overshoot of the absolute minimum energy configuration and may result in the fluid stabilizing in a relative minimum energy configuration.

7. Tankage system that utilizes surface tension for propellant positioning and/or mass transfer appears particularly attractive for the electric engines. Systems of this type should be developed for this application.

LIST OF REFERENCES

1. Electrothermal Engine Propellant Storage and Feed System Study, Phase II Report, Engineering Report No. 13558, Contract NAS-8-2574, Beech Aircraft Corporation. September 1962.

2. Fuel Feed Systems for Arc Jet Engines, Report No. ER-4821, Final Report on Contract NAS-8-2526, Thompson Ramo Wooldridge, Inc. March 1962.

3. Analysis of Cryogenic Propellant Feed Systems for Electrothermal Engines, Summary Report, Contract NAS-8-1962, Air Products and Chemicals, Inc. October 1961.

4. Research and Development of Lithium and Lithium Hydride Propellants Feed Systems for Electric Propulsion Systems, Summary Report, Contract NAS-8-2529, MSA Research Corporation. 27 June 1962.

5. Investigations of Propellant Feed Systems for Electrothermal Engines, Final Report, Contract NAS-8-1695, Arthur D. Little, Inc. October 1961.

6. Cryogenic Propellant Feed Systems for Electrcthermal Engines, Report No. AE-1952-R, Contract NAS-8-1694, Airesearch Manufacturing Divicion. 3 November 1961.

7. Cesium Ion Engine Propellant Feed System, Summary Report, Contract NAS-8-1621, Dresser Industries, Inc. 20 November 1961.

8. Research and Development of Propellant Feed System for Ion Engine, Summary Report, Contract NAS-8-1620, Rocketdyne. November 1961.

9. Propellant Feed Systems for Ion Engines: The Cesium Hydride System, Summary Report, Contract NAS-8-1616, Kelsey-Hayes Company. 15 February 1962.

10. Research and Development of Propellant Feed Systems for Ion Engines, Summary Report, Contract NAS-8-1617, MSA Research Corporation. 6 September 1961.

11. Research and Development of Propellant Feed Systems for Ion Engines, Summary Report, Contract NAS-8-1619, National Research Corporation. 30 September 1961.

12. Study of Feed System for Cesium Ion Engines, Summary Report, Contract NAS-8-1614, Aerojet-General Nucleonics. October 1961.

13. Research and Development of Propellant Feed Systems for Ion Engines, Final Report, Contract NAS-8-1615, General Electric Company. 16 September 1961.

14. Cesium Ion Propellant Feed System, Report No. ER-4619, Contract NAS-8-1618, Thompson Ramo Wooldridge, Inc. September 1961.

15. Cesium Ion Propellant System, ASD-TN-61-662, Prepared by Thompson Ramo Wooldridge, Inc., on Contract AF33(616)-7219, for Aeronautical Systems Division, Wright-Patterson Air Force Base, Ohio. 29 December 1961.

LIST OF REFERENCES (Continued)

16. Applied Research on Contact Ionization Thruster, Contract AF33(657)-8157, Electro-Optical Systems, Inc. March 1963.

17. Reynolds, W. C., Hydrodynamic Considerations for the Design of Systems for Very Low Gravity Environments, Technical Report LG-1, Stanford University. 1 September 1961.

18. Li, Ta, Dr., Hydrostatics in Various Gravitational Fields, General Dynamics/ Astronautics.

19. Benedikt, Elliot T., Epihydrostatics of a Liquid in a Rectangular Tank With Vertical Walls, ASL-TM-60-38, Northrop Corporation, Norair Division. November 1960.

20. Adamson, Arthur W., Physical Chemistry of Surfaces, Interscience Publishers, Inc. 1960.

21. Petrash, D. A., and Otto, E. W., Studies of the Liquid-Vapor Interface Configuration in Weightlessness, Prepared by Lewis Research Center, NASA for American Rocket Society Space Power Systems Conference. 25-28 September 1962.

22. Development of Expulsion and Orientation Systems for Advanced Liquid Rocket Propulsion Systems, Contract AF04(611)-8200, Bell Aerosystems Company. October 1962.

23. Niener, J. J., The Effect of Zero Gravity on Fluid Behavior and System Design, WADD-TN-59-149, ASTIA Document AD-215428, Propulsion Laboratory, Aeronautical Systems Division, Wright-Patterson Air Force Base, Ohio, April 1959.

24. Truselo, R. A., Captain, and Clodfelter, R. G., Heat Transfer Problems of Space Vehicles Power Systems, SAE Aeronautical Meeting, New York, New York. 5-8 April 1960.

25. Clodfelter, R. G., and Lewis, R. C. 1/Lt, Fluid Studies in a Zero Gravity Environment, ASD-TN-61-84, Propulsion Laboratory, Aeronautical Systems Division, Wright-Patterson Air Force Base, Ohio. June 1961.

26. Hobrock, Lowell M., Liquid Contact Angle Measurement, ASD Flight and Engineering Test Report, ASTEP 62-50R, Directorate of Engineering Test, Aeronautical Systems Division, Wright-Patterson Air Force Base, Ohio. 29 August 1962.